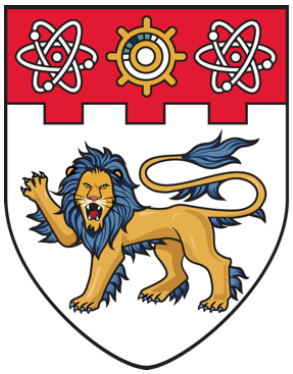

NANYANG TECHNOLOGICAL UNIVERSITY
SINGAPORE

VOLTAMMETRIC CURRENT AMPLIFICATION OF BISPHENOL A, AND ELECTROCHEMICAL CHARACTERISATION ANALYSIS OF CORANNULENE BASED COMPOUNDS AS ELECTRON ACCEPTORS

ZHOU JINGSONG

SCHOOL OF CHEMISTRY, CHEMICAL ENGINEERING AND BIOTECHNOLOGY

2025

VOLTAMMETRIC CURRENT AMPLIFICATION OF BISPHENOL A, AND ELECTROCHEMICAL CHARACTERISATION ANALYSIS OF CORANNULENE BASED COMPOUNDS AS ELECTRON ACCEPTORS

ZHOU JINGSONG

SCHOOL OF CHEMISTRY, CHEMICAL ENGINEERING AND BIOTECHNOLOGY

A thesis submitted to the Nanyang Technological University in partial fulfilment of the requirement for the degree of Master of Science

Statement of Originality

I hereby certify that the work embodied in this thesis is the result of original research, is free of plagiarised materials, and has not been submitted for a higher degree to any other University or Institution.

23/11/2025

. . . . . .

Date

. . . . . .

Zhou Jingsong

Supervisor Declaration Statement

I have reviewed the content and presentation style of this thesis and declare it is free of plagiarism and of sufficient grammatical clarity to be examined. To the best of my knowledge, the research and writing are those of the candidate except as acknowledged in the Author Attribution Statement. I confirm that the investigations were conducted in accord with the ethics policies and integrity standards of Nanyang Technological University and that the research data are presented honestly and without prejudice.

23/11/2025

. . . . . .

Date

. . . . . .

Richard D. Webster

Authorship Attribution Statement

This thesis contains material from **1** paper published in the following peer-reviewed journal in which I am listed as a co-author.

Chapter 5 is published as: J. Stanojkovic, R. Wiliiam, Z. Zhang, I. Fernández, J. Zhou, R.D. Webster, and M.C. Stuparu. Synthesis of precisely functionalizable curved nanographenes via graphitization-induced regioselective chlorination in a mechanochemical Scholl Reaction. *Nature Communications* ***14*****(1)**, *p.*803 (2023).

The contributions of the co-authors are as follows:

- A/Prof Stuparu designed the synthesis of the corannulene compounds and supervised the progress of the project.
- A/Prof Webster designed the electrochemical studies and experiments.
- Stanojkovic, Dr. Wiliiam, and Dr. Zhang performed material synthesis, molecule characterization and formulated data figures.
- I carried out the electrochemical experiments and the related laboratory work in the School of Chemistry, Chemical Engineering and Biotechnology.
- I analyzed the data and formulated figures and drafts for the section "Electrochemical Properties" in the manuscript. The final draft was revised by A/Prof Stuparu and A/P Webster.
- Prof Fernández carried out all the computational studies and wrote the theoretical part of the manuscript.

23/11/2025

. . . . . .

Date

. . . . . .

Zhou Jingsong

Acknowledgement

I wish to express my profound thanks to NTU and CCEB for the invaluable scholarship that funded my master's degree. My utmost gratitude goes to my exceptional supervisor, Associate Professor Richard Webster, where his expert guidance, constant support, and incredible patience were fundamental to navigating my project successfully. I feel immensely privileged to have had such an inspiring and understanding mentor.

Heartfelt thanks to my fantastic lab mates for their unwavering advice and support which was essential to my journey. To my long term lab partner, Cher , I am incredibly grateful for your patient tutelage during my early challenges with electrochemistry; your help was indispensable. Our engaging discussions were both enjoyable and highly productive. Kendrick, sincere thanks for your dedicated accompany and support during this journey. To all my undergraduate students, graduating or graduated – thank you for making our lab such a supportive, friendly, and truly enjoyable workplace. Working with you all has been a memorable and enriching experience that I will always cherish.

Finally, I would like to thank all the administrative officers for their support in processing and advising my thesis submission process. It was greatly appreciated.

Table of Contents

Abstract

Electrochemical analysis methods are effective in giving responsive and accurate characterization of organic molecules. This can be achieved through examining the changes in current (vertical axis) or shifts in potential (horizontal axis). In this work, these electrochemical analysis techniques were used to analyze signal responses of Bisphenol A (BPA) and functionalized corannulene compounds under the influence of current and voltage. It was found that the anodic current signals from BPA when performing Cyclic Voltammetry (CV) analysis showed large amplification (>13 fold), upon using a modified glassy carbon electrode drop-casted with a combination of magnetite nanoparticles (Fe_3O_4), functionalized multi-walled carbon nanotubes (f-MWCNTs) and polyvinylpyrrolidone (PVP). On the other hand, a cyanno-functionalised corannulene compound displayed especially high electron affinity (low reduction potential) paired with high chemical stability in their reduced states upon carrying out CV analysis. It was also observed that the reduced radical anion state of the cyanno-corannulene has high stability evident by in-situ electrospectroscopy and the radical anion is further confirmed using electron paramagnetic resonance (EPR) spectroscopy.

Chapter 1

Introduction

1.1 Background information on electrochemical methods for characterization

1.2 Background information on Bisphenol A and current amplification

1.3 Background information on corannulene compounds as electron acceptors

1.4 Objectives and Scope

1.5 References

1.1 Background information on electrochemical characterization

Electrochemical analysis using methods such as Cyclic voltammetry (CV), square-wave voltammetry (SWV), electrolysis and in-situ electrospectroscopy have been effective analytical methods in fields such as food safety[1], environmental security[2] and biomedical diagnostics[3]. It quantifies chemical species by measuring electrical signals (*current*, *potential*, *charge*, or *impedance*) arising from redox reactions at an electrode–solution interface[4]. These signals change or vary depending on the surrounding environment of the analytical sample such as the type of solvent systems[5], concentration of the analyte[5], or the type of material used as electrode surface[6].

In the first part of this thesis, CV was used to measure the current differences of Bisphenol A between using glassy carbon electrodes (GCE) and modified GCE surface electrodes drop-casted with a combination of magnetite nanoparticles (Fe_3O_4), functionalized multi-walled carbon nanotubes (f-MWCNTs) and polyvinylpyrrolidone (PVP). This system increases the diffusion rate of the analyte towards the electrode surface and the Iron NPs serve as a catalyst to regenerate analytes at the same time to achieve signal amplification, which could be crucial for application purposes such as detection in the future.

Electrochemical analysis using CV and SWV are also useful in analysing electron accepting/donating capabilities[7-8] by examining and comparing the different redox potentials of the analytes, as well as the stability of the redox forms based on the reversibility of the CV peaks[9-10]. For an electrochemically reversible process (fast electron transfer) the oxidative peak current (i_p^{ox}) to the reductive peak current (i_p^{red}) ratio (i_p^{ox}/i_p^{red}) measured by CV is an indication of the chemical stability of the reduced species at a defined voltammetric scan rate. i_p^{ox}/i_p^{red}-values ≥ 0.97 indicate that the reduced species is completely stable[9] (does not decompose) on

the timescale of the experiment, whereas $i_p^{ox}/i_p^{red} < 0.97$ indicate chemical reactivity of instability of the reduced species, with values further from unity implying greater reactivity (**Figure 1**).

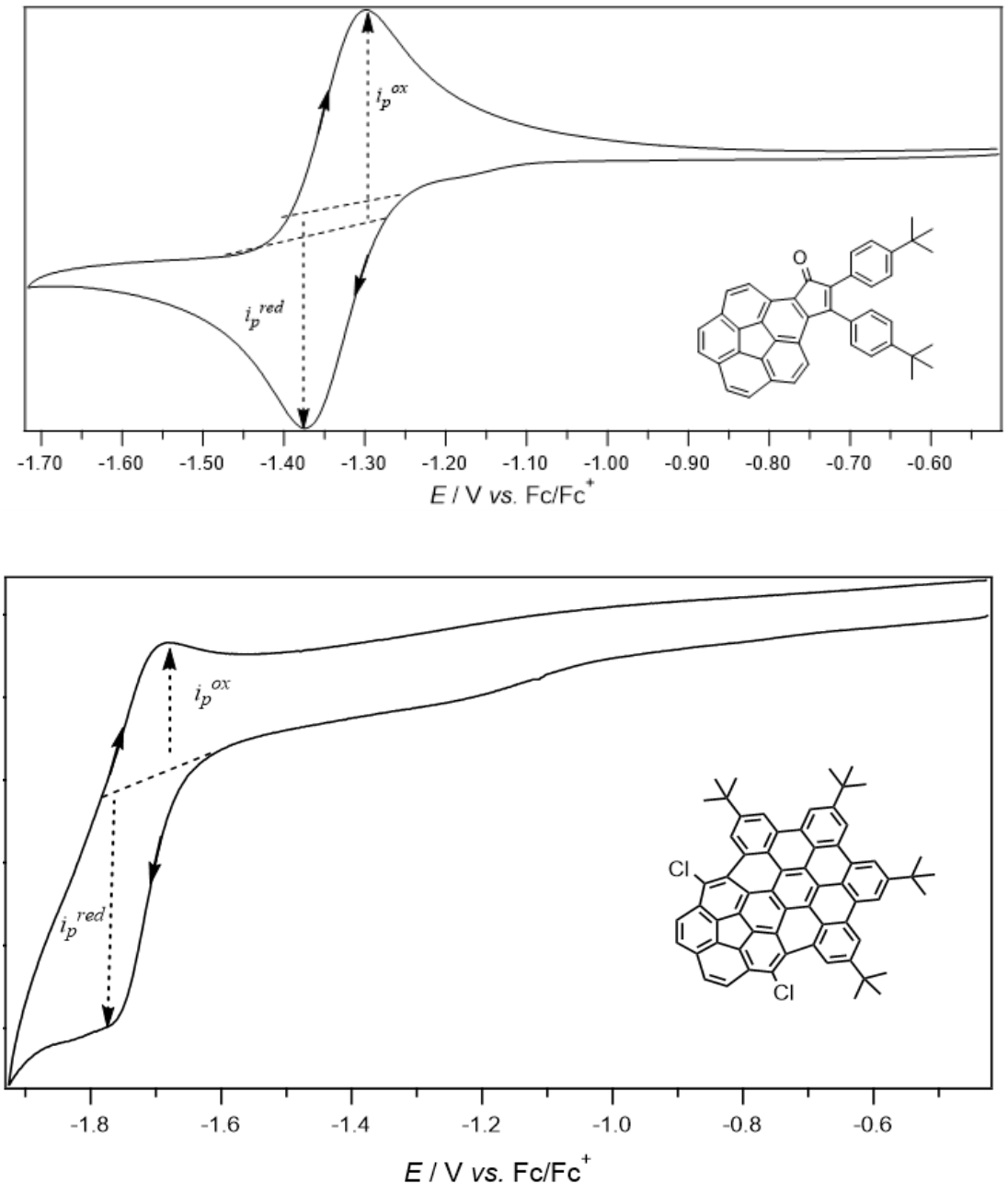

Figure 1. Illustration of electrochemical redox reversibility based on two corannulene compounds

This technique is extremely suitable for analyzing the electron accepting capability of corannulene based compounds and derivatives, as the first reduction potential and the stability of the reduced form are crucial properties defining the application potential of electron acceptors.

1.2 Background information on Bisphenol A and current amplification

Phenolic pollutants represent a major class of anthropogenic contaminants posing significant threats to human health[11-12], wildlife[13], and aquatic ecosystems[14]. Among these, Bisphenol A (BPA; 2,2'-bis(4-hydroxyphenyl)propane) stands out as one of the most pervasive and extensively manufactured phenolic poullutant[15-16]. BPA is a potent endocrine-disrupting chemical that is notorious for interfering with hormonal systems[15], and its exposure is linked to a wide array of serious health consequences, including immune dysfunction[17], reproductive disorders[18], metabolic diseases[19], and an elevated risk of certain cancers[20]. Furthermore, BPA's environmental persistence and ability to bioaccumulate[21] amplify its ecological damage, disrupting aquatic life reproduction, development and survival[14].

The sheer scale of BPA use in manufacturing polycarbonate plastics and epoxy resins found in food/drink containers, packaging[22], and medical devices[23] create continuous pathways for its release. Leaching occurs during product use, disposal and recycling processes. As such, the development of highly sensitive, rapid, and environmentally sustainable detection methods is urgent to enable effective monitoring, targeted removal, and ultimately, the mitigation of BPA's multifaceted risks.

Electrochemically, BPA exhibits a non-reversible 4 electron oxidation process as illustrated in **Figure 2**:

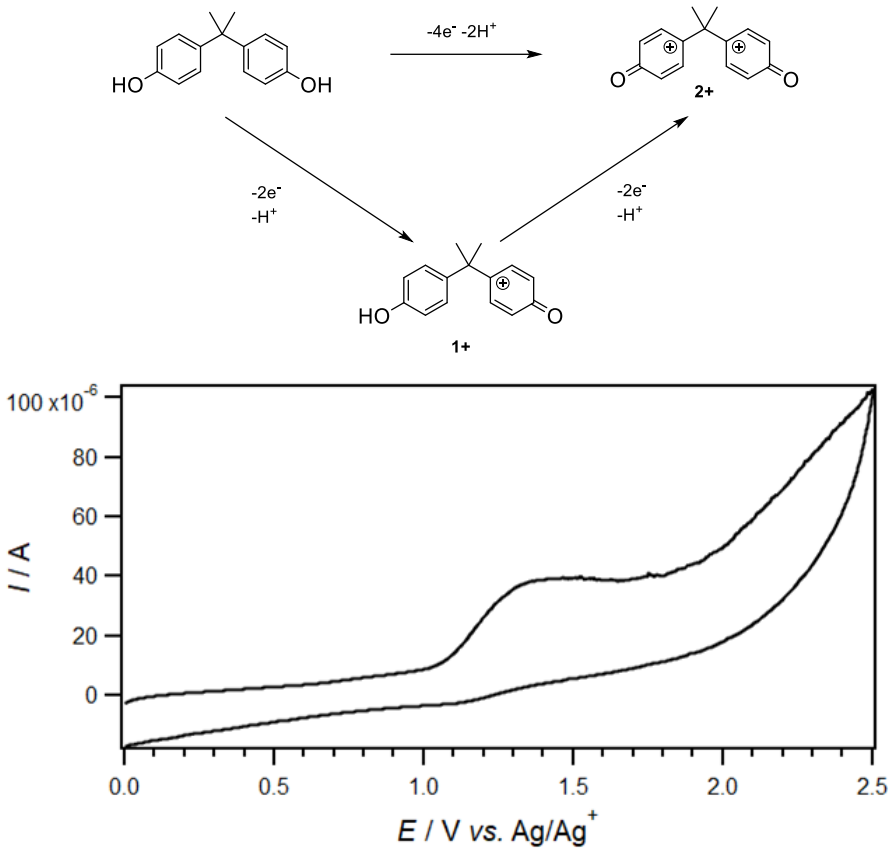

Figure 2. Illustration of stepwise oxidation process of BPA and the respective cyclic voltammogram.

Electrochemical studies detailed in literature[24] reveal that Bisphenol A (BPA) undergoes a characteristic oxidation process in acetonitrile when using an unmodified glassy carbon electrode (GCE). This process involves the net transfer of four electrons and two protons (a $4e^-/2H^+$ reaction). According to literature mechanistic analysis[24], supported by comparisons to similar mono-phenolic compounds indicates that this overall oxidation occurs via two sequential electrochemical steps. Each step is a 2-electron, 1-proton ($-2e^-/-H^+$) oxidation. The first oxidation step generates a highly unstable cationic intermediate species 1^+, which possesses an extremely short lifetime which causes electrochemical irreversibility.

1.3 Background information on corannulene compounds as electron acceptors

Electron affinity (EA) and efficient electron capture kinetics constitute fundamental material properties critically governing the performance of organic photovoltaic (OPV) devices, particularly within the bulk heterojunction (BHJ) architecture[25-26] essential for exciton dissociation and charge separation[26-27]. Conventionally, fullerene derivatives—notably phenyl-C_{61}-butyric acid methyl ester ($PC_{61}BM$) and phenyl-C_{71}-butyric acid methyl ester ($PC_{71}BM$)[28-30]—have dominated as the electron acceptor (n-type) materials in high-performance OPV systems due to several intrinsic advantages such enabling efficient electron transfer from donor polymers and subsequent isotropic charge percolation[31]. Additionally, fullerenes undergo multiple, electrochemically reversible reductions, demonstrating exceptional stability as radical anions[32] and tolerance to multiple electron occupation states[33], a key requirement for efficient charge transport.

However, significant limitations impede the further development and large-scale deployment of fullerene-based acceptors. Which includes restricted synthetic tunability[34], where modifying frontier molecular orbital energies (HOMO/LUMO) through chemical functionalization is challenging. Consequently, intensive research focuses on developing high-performance non-fullerene electron acceptors (NFAs) capable of matching or exceeding the power conversion efficiencies (PCEs) achieved with fullerenes. In this work, corannulene ($C_{20}H_{10}$) and its derivatives represent a highly promising class of NFAs. These polycyclic aromatic hydrocarbons (PAHs) possess a distinctive bowl-shaped structure with inherent Gaussian curvature, which induces significant intrinsic electron affinity, enabling efficient electron accepting capabilities comparable to some fullerenes. Furthermore, the readily accessible peripheral positions of the corannulene core offer enhanced synthetic tunability[35], allowing precise modulation of solubility, solid-state packing and frontier orbital energetics

(HOMO/LUMO levels)[36]. This tunability offers pathways to overcome the key limitations of fullerenes.

The first electrochemically reversible reduction potential (Er) serves as a critical quantitative indicator of a compound's electron affinity (EA)[37], directly reflecting the standard Gibbs free energy change associated with the single-electron reduction process[38]. A less negative (more positive) Er_1 signifies a lower energetic barrier and greater thermodynamic driving force for electron uptake[37]. Strategic molecular engineering through peripheral functionalization of corannulene with strong electron-withdrawing groups (EWGs) – such as cyano (-CN), Keto, (=O) dicyanomethylene ($=C(CN)_2$), or fluorinated moieties effectively lowers its lowest unoccupied molecular orbital (LUMO) energy. This LUMO stabilization manifests as an anodic shift (less negative value) in Er_1, thereby enhancing EA towards levels competitive with fullerene derivatives. demonstrating the pivotal role of targeted synthesis in optimizing electron-accepting materials (**Figure 3**).

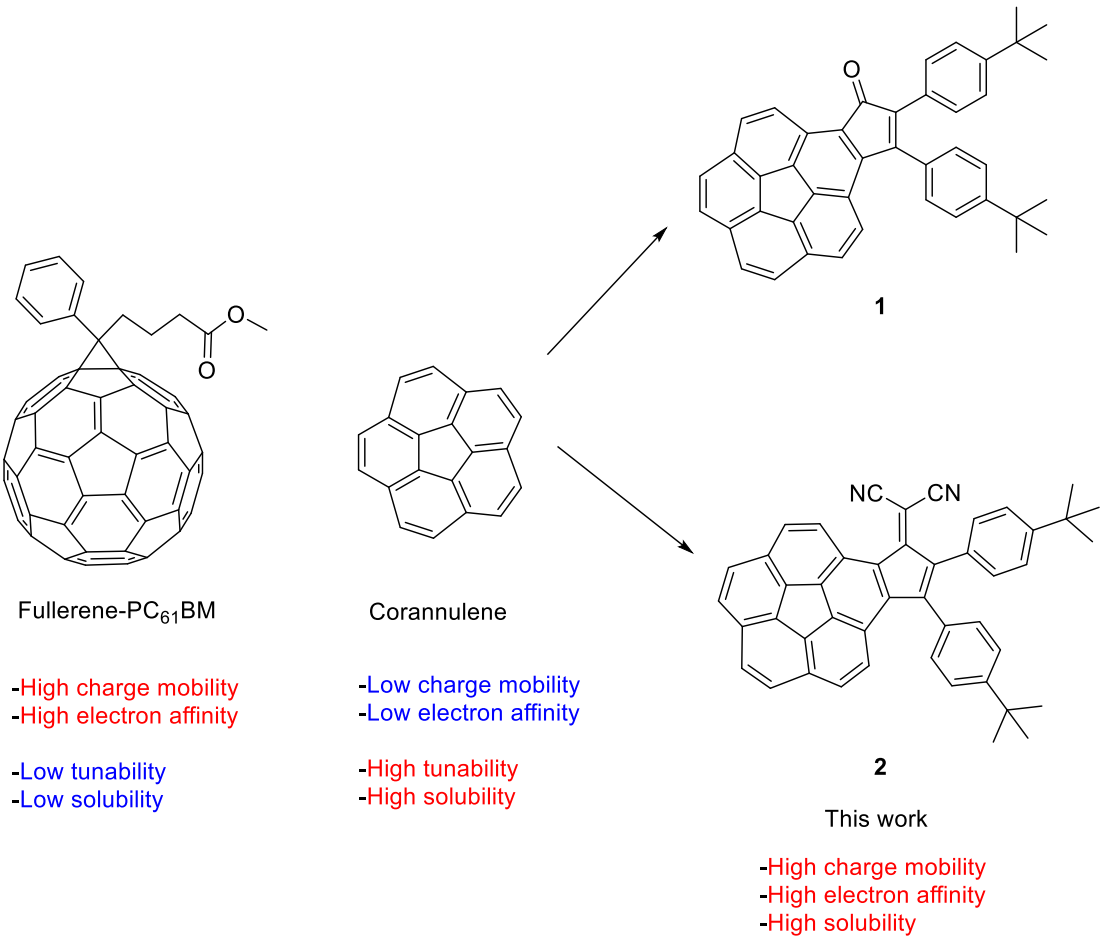

Figure 3. Optimization of electron accepting capability using corannulene base compounds through synthetic functionalization.

1.4 Objectives and Scope

This project seeks to enhance the electrochemical detection sensitivity for the environmental contaminant Bisphenol A (BPA) by engineering a modified carbon paste electrode surface. This involves fabricating a nanocomposite-modified glassy carbon electrode (GCE) using magnetite nanoparticles (FeNPs), functionalized multi-walled carbon nanotubes (f-MWCNTs), and polyvinylpyrrolidone (PVP), and evaluating its performance against an unmodified GCE. The modification strategy targets signal amplification through enhanced mass transport of the analyte to the electrode interface and electrocatalytic regeneration of BPA mediated by the Fe_3O_4 NPs.

Additionally, this project aims to characterize the electron-accepting capability and stability of reduced species of corannulene-based compounds and their derivatives. This involves determining key parameters such as the first reduction potential and assessing the chemical stability of the electrogenerated species.

The project scope focuses on electrode modification and sensor development for BPA using Cyclic Voltammetry (CV) as the primary technique to quantify current response differences between bare GCE and the modified GCE and examines the impact of the nanocomposite on the electrode-solution interface dynamics, including analyte diffusion and catalytic processes. On the other hand, the corannulene project employs Cyclic Voltammetry (CV) and Square-Wave Voltammetry (SQW) for the redox characterization of corannulene derivatives. electrochemical reversibility based on CV peak separation and chemical stability of the reduced forms via the ratio of anodic to cathodic peak currents are also investigated. On top of that, in-situ electrospectrosocpy is employed to investigate the lifetime of the reduced species of the corannulene derivatives, informing the compounds' suitability as electron-accepting materials.

1.4 References

1. Li, F.; Yu, Z.; Han, X.; Lai, R. Y Electrochemical aptamer-based sensors for food and water analysis: A review. *Anal. Chim. Acta.* **2019**, *1051*, 1–23.

2. Gumpu, M. B.; Sethuraman, S.; Krishnan, U. M.; Rayappan, J. B. B. A review on detection of heavy metal ions in water – An electrochemical approach. *Sens. Actuators. B*. **2015**, *213*, 515–533.

3. Dai, Y.; Wu, Y.; Liu, G.; Gooding, J. J. CRISPR Mediated Biosensing Toward Understanding Cellular Biology and Point-of-Care Diagnosis. *Angew. Chem. Int. Ed*. **2020**, *59* (47), 20754–20766.

4. Marken, F.; Neudeck, A.; Bond, A. M. Cyclic voltammetry. *Electroanalytical methods.* **2010,** 57-106.

5. Elgrishi, N.; Rountree, K. J.; McCarthy, B. D.; Rountree, E. S.; Eisenhart, T. T.; Dempsey, J. L. A practical beginner's guide to cyclic voltammetry. *J. Chem. Educ.* **2018,** *95*(2), 197-206.

6. Yamada, H.; Yoshii, K.; Asahi, M.; Chiku, M.; Kitazumi, Y. Cyclic voltammetry part 1: fundamentals. *Electrochem.* **2022.** *90*(10), 102005-102005.

7. Fricke, K.; Harnisch, F.; Schröder, U. On the use of cyclic voltammetry for the study of anodic electron transfer in microbial fuel cells. *Energy Environ. Sci.* **2008.** *1*(1), 144-147.

8. Nagaraja, C.; Venkatesha, T. V. The influence of electron donating tendency on electrochemical oxidative behavior of hydroquinone: Experimental and theoretical investigations. *Electrochim. Acta*. **2018.** *260*, 221-234.

9. Heinze, J. Cyclic voltammetry—“electrochemical spectroscopy”. New analytical methods (25). *Angew. Chem. Int. Ed.* **1984.** *23*(11), 831-847.

10. Bilal, S. Cyclic voltammetry. *Encyclopedia of applied electrochemistry* **2014.** 285-289. Springer, New York, NY.

11. Vermerris, W.; Nicholson, R.; Vermerris, W.; Nicholson, R. Phenolic compounds and their effects on human health. **2006.** 235-255. Springer Netherlands.

12. Ozcan, T.; Akpinar-Bayizit, A.; Yilmaz-Ersan, L.; Delikanli, B. Phenolics in human health. *Int. J. Chem.Eng. Appl.* **2014.** *5*(5), 393-396.

13. Bodziach, K.; Staniszewska, M.; Falkowska, L.; Nehring, I.; Ożarowska, A.; Zaniewicz, G.; Meissner, W. Gastrointestinal and respiratory exposure of water birds to endocrine disrupting phenolic compounds. *Sci. Total Environ*, **2021.** *754*, 142435.

14. Park, J. S.; Brown, M. T.; Han, T. Phenol toxicity to the aquatic macrophyte Lemna paucicostata. *Aquat. Toxicol.* **2012.** *106*, 182-188.

15. Vom Saal, F. S.; Vandenberg, L. N. Update on the health effects of bisphenol A: overwhelming evidence of harm. *Endocrinol*. **2021.** *162*(3), bqaa171.

16. Hahladakis, J. N.; Iacovidou, E.; Gerassimidou, S. An overview of the occurrence, fate, and human risks of the bisphenol-A present in plastic materials, components, and products. *Integr Environ. Asses.* **2023.** *19*(1), 45-62.

17. Pirozzi, C.; Lama, A.; Annunziata, C.; Cavaliere, G.; Ruiz-Fernandez, C.; Monnolo, A.; Meli, R. Oral bisphenol A worsens liver immune-metabolic and mitochondrial dysfunction induced by high-fat diet in adult mice: cross-talk between oxidative stress and inflammasome pathway. *Antioxidants*, **2020.** *9*(12), 1201.

18. Meli, R. Monnolo, A. Annunziata, C. Pirozzi, C. Ferrante, M. C. Oxidative stress and BPA toxicity: an antioxidant approach for male and female reproductive dysfunction. *Antioxidants*, **2020.** *9*(5), 405.

19. Hwang, S.; Lim, J. E.; Choi, Y.; Jee, S. H. Bisphenol A exposure and type 2 diabetes mellitus risk: a meta-analysis. *BMC Endocr. Disord.* **2018.** *18*, 1-10.

20. Yang, M.; Ryu, J. H.; Jeon, R.; Kang, D.; Yoo, K. Y. Effects of bisphenol A on breast cancer and its risk factors. *Arch. Toxicol.* **2009.** *83*, 281-285.

21. Corrales, J.; Kristofco, L. A.; Steele, W. B.; Yates, B. S.; Breed, C. S.; Williams, E. S.; Brooks, B. W. Global assessment of bisphenol A in the environment: review and analysis of its occurrence and bioaccumulation. *Dose-response*. **2015.** *13*(3), 1559325815598308.

22. Khalili Sadrabad, E.; Hashemi, S. A.; Nadjarzadeh, A.; Askari, E.; Akrami Mohajeri, F.; Ramroudi, F. Bisphenol A release from food and beverage containers–A review. *Food Sci. Nutr.* **2023.** *11*(7), 3718-3728.

23. Guimarães, A. G. C.; Coutinho, V. L.; Meyer, A.; Lisboa, P. C.; de Moura, E. G. Human exposure to bisphenol A (BPA) through medical-hospital devices: a systematic review. *Environ. Toxicol. Pharmacol*. **2023.** *97*, 104040.

24. Chan, Y. Y.; Yue, Y.; Li, Y.; Webster, R. D. Electrochemical/chemical oxidation of bisphenol A in a four-electron/two- proton process in aprotic organic solvents. *Electrochim. Acta.* **2013**, *112*, 287–294.

25. Facchetti, A. Polymer donor–polymer acceptor (all-polymer) solar cells. *Materials Today*, **2013.** *16*(4), 123-132.

26. Blom, P. W., Mihailetchi, V. D., Koster, L. J. A., Markov, D. E. *Adv. Mater.* **2007**, *19*(12), 1551-1566.

27. Cha, H.; Fish, G.; Luke, J.; Alraddadi, A.; Lee, H. H.; Zhang, W.; Durrant, J. R. Suppression of recombination losses in polymer: nonfullerene acceptor organic solar cells due to aggregation dependence of acceptor electron affinity. *Adv. Energy Mater*. **2019.** *9*(27), 1901254.

28. Liu, T.; Troisi, A. What makes fullerene acceptors special as electron acceptors in organic solar cells and how to replace them. *Adv. Mater*. **2013**, *25*(7), 1038-1041.

29. Ganesamoorthy, R.; Sathiyan, G.; Sakthivel, P. Fullerene based acceptors for efficient bulk heterojunction organic solar cell applications. *Sol. Energy Mater. Sol. Cells*. **2017.** *161*, 102-148.

30. Akaike, K.; Kumai, T.; Nakano, K.; Abdullah, S.; Ouchi, S.; Uemura, Y.; Kanai, K. Effects of molecular orientation of a fullerene derivative at the donor/acceptor interface on the device performance of organic photovoltaics. *Chem. Mater.* **2018.** *30*(22), 8233-8243.

31. Ford, M. J.; Wang, M.; Bustillo, K. C.; Yuan, J.; Nguyen, T. Q.; Bazan, G. C. Acceptor Percolation Determines How Electron-Accepting Additives Modify Transport of Ambipolar Polymer Organic Field-Effect Transistors. *ACS nano*. **2018.** *12*(7), 7134-7140.

32. Liu, D.; Nagamori, T.; Yabusaki, M.; Yasuda, T.; Han, L.; Marumoto, K. Dramatic enhancement of fullerene anion formation in polymer solar cells by thermal annealing: Direct observation by electron spin resonance. *Applied physics letters*. **2014.** *104*(24).

33. Liu, T. Troisi, A. Absolute rate of charge separation and recombination in a molecular model of the P3HT/PCBM interface. *J. Phys. Chem. C*. **2011.** *115*(5), 2406-2415.

34. Chen, H.; Peet, J.; Hu, S.; Azoulay, J.; Bazan, G.; Dadmun, M. The Role of Fullerene Mixing Behavior in the Performance of Organic Photovoltaics: PCBM in Low-Bandgap Polymers. *Advanced Functional Materials*. **2014.** *24*(1), 140-150.

35. Stuparu, M. C. Corannulene: a curved polyarene building block for the construction of functional materials. *Acc. Chem. Res*. **2021.** *54*(13), 2858-2870.

36. Sanyal, S.; Manna, A. K.; Pati, S. K. Functional corannulene: diverse structures, enhanced charge transport, and tunable optoelectronic properties. *ChemPhysChem*. **2014.** *15*(5), 885-893.

37. Calbo, J.; Viruela, R.; Ortí, E.; Aragó, J. Relationship between electron affinity and half-wave reduction potential: a theoretical study on cyclic electron-acceptor compounds. *ChemPhysChem*. **2016.** *17*(23), 3881-3890.

38. Campero, A.; Díaz Ponce, J. A. Relationship between the Atomic Structure and Electrochemistry. 1. Electric Force, Standard Reduction Potential E°, and Standard Reaction Gibbs Free Energy Δ G°. *ACS omega*. **2020.** *5*(21), 12046-12056.

Chapter 2

Literature Review

2.1 Overview

2.2 Modification of electrode for current amplification

2.3 Current advances and methods in detection of BPA

2.4 Electron accepting properties of corannulene based compounds

2.5 Research gaps

2.6 References

2.1 Overview

Electrochemical analysis techniques provide a highly effective methodology for the quantitative interrogation and characterization of organic molecular species, offering exceptional temporal resolution and sensitivity to redox-active functionalities[1]. The measured current (*i*) is directly proportional to the rate of the heterogeneous electron transfer reaction occurring at the electrode-solution interface, governed by Faraday's Law[2]:

$$i = nF\frac{dN}{dt}$$

where *n* is the number of electrons transferred per molecule, *F* is the Faraday constant (96,485 C mol^{-1}), and dN/dt is the rate of conversion of reactant molecules (mol s^{-1}).

Observed shifts in the characteristic potential (*E*) of redox events, such as the peak potential (*Ep*) in cyclic voltammetry, are primarily dictated by the Nernst Equation for reversible systems, reflecting the thermodynamic driving force[3]:

$$E = E^{o} - \frac{RT}{nF}\ln\left(\frac{[Red]}{[Ox]}\right)$$

where *E*∘ is the formal potential, *R* is the universal gas constant (8.314 J mol^{-1} K^{-1}), *T* is the absolute temperature (K), and [Red]/[Ox] is the ratio of reduced to oxidized species concentrations near the electrode.

Within this experimental framework, present studies employ potentiodynamic techniques, notably cyclic voltammetry[4] (CV) and Square-wave voltammetry[5] (SWV), to systematically investigate the electrochemical signal responses generated by Bisphenol A (BPA) and synthetically functionalized corannulene derivatives.

For BPA, the analytical signal arises predominantly from the irreversible, diffusion-controlled oxidation of its phenolic moieties. The peak current (i_p) scales linearly with concentration, governed by the Randles-Sevcik equation:

$$i_p = (2.69 \times 10^5) n^{3/2} A C D^{1/2} v^{1/2}$$

where A is the electrode area (cm^2), D is the diffusion coefficient ($cm^2\ s^{-1}$), v is the scan rate ($V\ s^{-1}$), and n is the number of electrons transferred in the rate-determining step.

On the other hand, functionalized corannulenes, particularly those with extended π-systems or redox-active substituents, exhibit distinct, often multi-electron, quasi-reversible or reversible redox properties[6-8]. The position of the voltage potential (E_p) where resulting current peak occurs indicates the energy level properties of these compounds, including HOMO-LUMO energy gaps approximated from the onset potentials, and the thermodynamic stability of various oxidized/reduced states.

2.2 Modification of electrode surface for current amplification

Many current works from other literatures focus on improving the rate of diffusion of BPA analyte to the electrode surface (*D*) either by increasing the conductivity or surface area[9-11] (*A*) of electrode surface, as according to the Randles-Sevcik equation. For example, many studies have made used of nanoparticles[9], transition metal species[9], or electrocatalytic materials[11] to coat onto the electrode surface. These modified electrode leverages effects such as:

1. Analytes adsorb onto high-surface-area nanostructures[9].
2. Electrocatalytic sites oxidize BPA at lower potentials[12].
3. Electrons transfer rapidly via conductive pathways to the electrode[10,13].

For more visualized examples, Thamilselvan *et. al.* employs the use of gold nanoparticles paired with MWCNTs to fabricate GCE surface[10], to essentially increase the surface area of active sites, and to provide more active sites on the electrode surface for BPA molecules to adsorb on. While Li and co-workers established an affinity-based chemical functionalization of the electrode surface using melamine to attract BPA through intermolecular attractions[13] (**Figure 4.**).

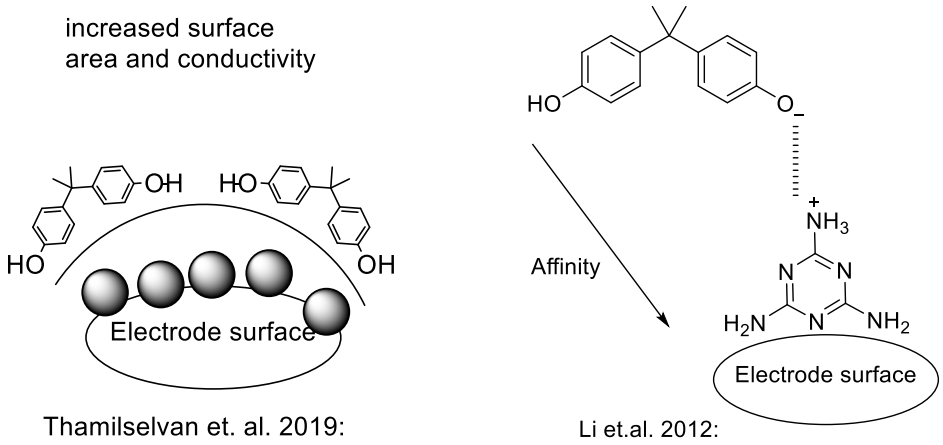

Figure 4. Illustration of two of the popular current strategies in enhancing current amplification in detection of BPA through electrochemistry

In the above cases, the degree of current amplification is limited by how fast new BPA molecules can diffuse from the bulk solution to the electrode surface to be oxidized. Once the molecules at the surface are oxidized, 'new' BPA molecules have to diffuse towards the surface again from the bulk solution for the oxidation process to continue, resulting in a direct correlation between oxidation peak height vs initial concentration of BPA molecules present. The catalytic regeneration of BPA mechanism in this project, however, utilizes a transition metal reductant Fe_3O_4 nanoparticles to reduce the chemically active oxidized BPA back to its neutral state after the oxidation process from electrode. This overcomes the need for fresh BPA molecules to diffuse to the electrode surface again and provides a constant accumulation of peak current, resulting in high enhancement of the peak current recorded.

2.3 Current advances and methods in detection of BPA

There are many other well established analytical methods alongside electrochemical sensors such as fluorescence detection[14], liquid chromatography-mass spectroscopy[15] (LCMS), gas chromatography-mass spectroscopy[16] (GCMS). Each method possesses merits and disadvantages of their own which are illustrated in **Table 1**, while electrochemical analysis methods stand out in terms of giving rapid real-time analysis, minimal sample preparation, cost-effectiveness, and robust *in-situ* applicability across complex matrices like biological fluids or environmental samples. Thus, supporting critical applications in biosensing, environmental monitoring, energy storage research, and mechanistic studies of molecular processes.

Table 1. Comparison between different methods of BPA detection.

	Electrochemistry	Fluorescence	LC-MS
Sensitivity (LOD)	~5.0pM (Carbon nanotube/ionic liquid/titania/Nafion/GCE) Jang et.al. 2016[17]	~0.9nM (zinc-based porphyrin metal-organic framework probe)[14] Pang et. al. 2022	~0.2nM (on-line SPE-UHPLC/MS/MS system)[15] Gely et. al. 2021
Pre-treatment	Addition of electrolyte salt required for reducing resistance of the analyte solution	Pristine BPA has low fluorescence efficiency. Addition of dyes and polymers as probes are usually needed	Run high purity mobile phase through the column for ~30min is required to equilibrate the machine

Time needed	Real-life determination, generate results within seconds	Real-life determination, generate results within seconds	Generates results within minutes (<10min)
Destructive of sample	Non-destructive	Non-destructive	Destructive
Interference and resolution	30mV-59.2mV peak to peak separation[18] (Electrochemical methods : fundamentals and applications by Allen J. Bard, Larry R. Faulkner)	10-15nm of wavelengths with interference filter[19]	1.1mDa~2.37mDa (high resolution mass spectroscpy *Anal. Chem.* 2012, 84, 2, 708–719)[20]

However, as much as electrochemistry can be an excellent portable analytical method, it still has its limitations. As compared to chromatographic techniques like LC-MS, electrochemistry can fall short when dealing with complex mixtures which require structural confirmation, or analyzing non-electroactive or trace-level compounds. For example, in the field of pharmaceutical and forensics toxicology, analysis of samples are often carried out in complex media such as body fluids. The presence of many other trace components could interfere by generating many overlapping electrochemical signals. For chromatographic tehcniques such as LC-MS, effective separation of the different components can be more effective in identifying molecules such as drugs in the samples. Fluorescence techniques can also potentially be more effective when targeting specific fluorescent compounds more specific and suitable than electrochemistry. In general, Electrochemistry provides information about redox behavior but does not offer structural or molecular mass data, and does not provide separational means.

2.4 Electron accepting properties of corannulene based compounds

An effective way to assess the electron affinity of the compounds is measuring their first electrochemically reversible reductive peak through voltammetry. For instance, the first formal reduction potential (E^0_f) of PCBM is around -0.90 V[21] while that of pristine corannulene is around -2.30V[22], with respect to the ferrocene/ferrocenium redox pair (Fc/Fc^+). This is an indication on how much, or rather how little energy is required for the compound to accept one single electron transfer. The most critical molecular design feature of fullerene-based acceptors like PCBM being able to dominate the field of electron acceptors is its closed, 3D cage and the resulting ultra-delocalized electron structure. This means that every carbon atom is sp^2 hybridized in the closed spherical/ellipsoidal molecule and enables a vast, continuous, and symmetric π-electron cloud over the entire surface of the molecule[23]. This feature effectively provides excellent electronic coupling between adjacent fullerene molecules allows for very fast "electron hopping."[23] On top of that, the rigid, spherical structure also leads to favorable packing in the solid state, minimizing energetic disorder and traps that could slow down charge carriers.

On the other hand, corannulene based molecules are curved[8], where the π-system is largely confined to a single, curved surface. In the solid state, these bowls tend to pack in a "ball-and-socket" fashion or in columns[8]. Electron transport is therefore anisotropic (direction-dependent). It is much more efficient within the plane of the π-stack than between stacks. This prevents the formation of the isotropic, 3D electron transport network that fullerenes provide effectively.

Whilst PCBM leads the field with the least negative reduction potential of sub -1.0 V *vs.* Fc/Fc^+ and excellent stability in its reduced state[24], modification of the corannulene structure with electron-withdrawing functional groups[25] has achieved significant enhancements to the

electron affinity of the aromatic nucleus in recent years[26]. For example, fluorinated corannulenes synthesized by Boltalina *et al.* [25], and bis-imides/cyano derivatives of Lentz *et al*[26] led to formal one-electron reduction potentials of -1.23 V and -1.42 V *vs.* Fc/Fc^{+}, respectively. While the corannulene with the highest anodic shift reported to date is by Stuparu *et al.* of a sulfone corannulene derivative[27] with an E^{0}_{f} = -1.10 V *vs.* Fc/Fc^{+}, (**Figure 5**) Although the improvement on the electron affinity of corannulene based compounds is huge, the range still falls short of PCBM which is 0.20 V more positive. However, the improvement is promising as it demonstrates the possibility and feasibility of using corannulene based compounds as a potential substituent for the expensive and less chemically tunable fullerene compounds.

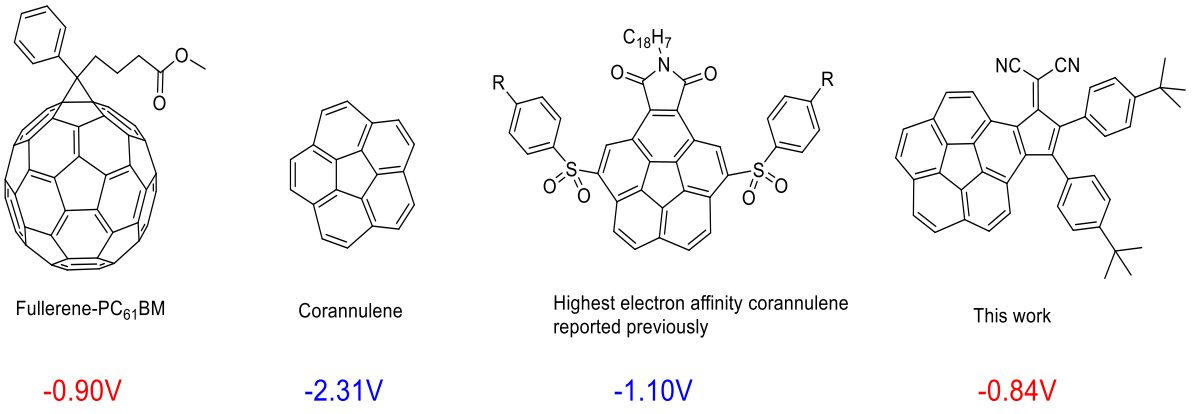

Figure 5. Comparison of the different first reduction potential of different corannulene compounds with PCBM

2.5 Research gap

2.5.1 Bisphenol A detection

Existing approaches to enhancing electrochemical detection sensitivity primarily focus on improving analyte diffusion to the electrode surface. This is achieved either by increasing electrode conductivity/surface area[10] (e.g., Thamilselvan et al., 2019) or by functionalizing the electrode surface with chemicals that attract the analyte[13] (e.g., Li et al., 2012). These strategies remain fundamentally constrained by diffusion-limited mass transport. The novelty of this thesis lies in proposing an alternative current amplification mechanism. Specifically, it hypothesizes the catalytic regeneration of the target analyte, Bisphenol A, immediately after its electrochemical oxidation, facilitated by a surface-bound reductant (FeNPs). This mechanism aims to circumvent the inherent limitation of solution-phase diffusion and to generate a high current amplification for low concentrations of BPA, which could be highly useful for the detection for extremely low concentrations of BPA.

2.5.2 Corannulene as electron acceptors

While significant progress has been made in enhancing the electron affinity of corannulene derivatives through strategic functionalization with electron-withdrawing groups, such as fluorine, bis-imides, cyano groups, and sulfones, these modified corannulenes consistently exhibit first reduction potentials that are substantially more negative (requiring more energy for reduction) than the benchmark fullerene acceptor PCBM. Even the most successful corannulene modification reported prior to this work, achieving a reduction potential of -1.10 V vs. Fc/Fc+, remained 0.20 V less positive (more negative) than PCBM's value of -0.90 V. This persistent gap highlighted a limitation in reaching the crucial electron affinity levels necessary for corannulenes to be considered truly competitive replacements for fullerenes like

PCBM in applications requiring high electron affinity, despite the promise shown in improving the inherent properties of the corannulene core.

This thesis presents the instance of a corannulene-based compound not only matching but exceeding the first reduction potential of PCBM, the most widely used fullerene acceptor. This demonstrates that corannulene derivatives can achieve electron affinities superior to this critical benchmark, a feat previously unrealized. The novelty is rigorously substantiated through comprehensive electrochemical characterization using cyclic voltammetry and square-wave voltammetry. Furthermore, the stability and nature of the reduced species are confirmed via in-situ electrolysis coupled with UV-vis spectroscopy, proving the chemical reversibility of the reduction process, and electron paramagnetic resonance (EPR) spectroscopy, which identifies the formation of the radical anion upon one-electron reduction. This represents a pivotal advancement in developing corannulene as a viable, high-performance, and synthetically tunable alternative to traditional fullerene acceptors.

2.6 References

1. Oja, S. M.; Wood, M.; Zhang, B. Nanoscale electrochemistry. *Anal. Chem*. **2013.** *85*(2), 473-486.

2 Piechota, E. J.; Meyer, G. J. Introduction to electron transfer: Theoretical foundations and pedagogical examples. *J. Chem. Educ*. **2019.** *96*(11), 2450-2466.

3. Vidal-Iglesias, F. J.; Solla-Gullón, J.; Rodes, A.; Herrero, E.; Aldaz, A. Understanding the Nernst equation and other electrochemical concepts: an easy experimental approach for students. *J. Chem. Educ*. **2012.** *89*(7), 936-939.

4. Tajik, S.; Beitollahi, H.; Nejad, F. G.; Zhang, K.; Le, Q. V.; Jang, H. W.; Shokouhimehr, M. Recent advances in electrochemical sensors and biosensors for detecting bisphenol A. *Sensors*. **2020.** *20*(12), 3364.

5. Gugoasa, L. A. D. electrochemical sensors for determination of the endocrine disruptor, bisphenol A. *J. Electrochem. Soc*. **2019.** *167*(3), 037506.

6. Wu, Y. L.; Stuparu, M. C.; Boudon, C.; Gisselbrecht, J. P.; Schweizer, W. B.; Baldridge, K. K.; Diederich, F. Structural, optical, and electrochemical properties of three-dimensional push–pull corannulenes. *The Journal of organic chemistry*. **2012.** *77*(24), 11014-11026.

7. Valenti, G.; Bruno, C.; Rapino, S.; Fiorani, A.; Jackson, E. A.; Scott, L. T.; Marcaccio, M. Intense and tunable electrochemiluminescence of corannulene. *J. Phys. Chem. C*. **2010.** *114*(45), 19467-19472.

8. Zhang, Z.; Csókás, D.; Fernández, I.; Stuparu, M. C. Chiral stacks of a curved nanographene. *Chem*. **2024.** *10*(10), 3199-3211.

9. Niu, X.; Yang, W.; Wang, G.; Ren, J.; Guo, H.; Gao, J. A novel electrochemical sensor of bisphenol A based on stacked graphene nanofibers/gold nanoparticles composite modified glassy carbon electrode. *Electrochim. Acta*. **2013.** *98*, 167-175.

10. Thamilselvan, A.; Rajagopal, V.; Suryanarayanan, V. Highly sensitive and selective amperometric determination of BPA on carbon black/f-MWCNT composite modified GCE. *J. Alloys Compd*. **2019.** *786*, 698-706.

11. Zhu, L.; Cao, Y.; Cao, G. Electrochemical sensor based on magnetic molecularly imprinted nanoparticles at surfactant modified magnetic electrode for determination of bisphenol A. *Biosens. Bioelectron.* **2014.** *54*, 258-261.

12. Wang, A., Wei, Y., & Wang, C. Study on the electrocatalytic oxidation of Bisphenol A on Au nanoparticles/carbon nanotubes composite modified electrode. *J. Anal. Chem*. **2015.** *70*(1), 67-71.

13. Li, Y., Gao, Y., Cao, Y., & Li, H. (2012). Electrochemical sensor for bisphenol A determination based on MWCNT/melamine complex modified GCE. *Sensors and Actuators B: Chemical*, *171*, 726-733.

14. Pang, Y.; Cao, Y.; Han, J.; Xia, Y.; He, Z.; Sun, L.; Liang, J. A novel fluorescence sensor based on Zn porphyrin MOFs for the detection of bisphenol A with highly selectivity and sensitivity *Food Control*, **2022**, *132*, 108551.

15. Gély, C. A.; Huesca, A.; Picard-Hagen, N.; Toutain, P. L,; Berrebi, A.; Gauderat, G.; Lacroix, M. Z. A new LC/MS method for specific determination of human systemic exposure to bisphenol A, F and S through their metabolites: Application to cord blood samples. *Environ. Int.* **2021**,*151*, 106429.

16. Becerra, V.; Odermatt, J. Detection and quantification of traces of bisphenol A and bisphenol S in paper samples using analytical pyrolysis-GC/MS. *Analyst*. **2012.** *137*(9), 2250-2259.

17. Jang, Junho,; Dong-Hwan Kim,; Won-Yong Lee. Electrochemical determination of bisphenol A by single-walled carbon nanotube composite glassy carbon electrode. *Ana.l Lett.* **2016.** 49, no. 13: 2018-2030.

18. Bard, A. J.; Faulkner, L. R.; White, H. S. *Electrochemical methods: fundamentals and applications*. **2022.** John Wiley & Sons.

19. Wehry, E. L. *Modern fluorescence spectroscopy*. **2012** Springer Science & Business Media.

20. Xian, F.; Hendrickson, C. L.; Marshall, A. G. High resolution mass spectrometry. *Anal. Chem*. **2012.** *84*(2), 708-719.

21. Yi, Z.; Ni, W.; Zhang, Q.; Li, M.; Kan, B.; Wan, X. Chen, Y. Effect of thermal annealing on active layer morphology and performance for small molecule bulk heterojunction organic solar cells. *J Mater. Chem. C*. **2014** *2*(35), 7247-7255.

22. Báti, G.; Csókás, D.; Yong, T.; Tam, S. M.; Shi, R. R.; Webster, R. D.; Stuparu, M. C. Mechanochemical Synthesis of Corannulene-Based Curved Nanographenes. *Angew. Chem., Int. Ed.* **2020.** *132*(48), 21804-21810.

23. Guldi, D. M.; Rahman, G. A.; Sgobba, V.; Ehli, C. Multifunctional molecular carbon materials—from fullerenes to carbon nanotubes. **2006.** *35(5) Chem. Soc. Rev*. 471-487.

24. Zimmermann, B.; Würfel, U.; Niggemann, M. Longterm stability of efficient inverted P3HT: PCBM solar cells. *Sol. Energy Mater. Sol. Cells*. **2009.** *93*(4), 491-496.

25. I. V. Kuvychko,; C. Dubceac,; S. H. M. Deng,;X.-B. Wang,; A. A. Granovsky,; A. A. Popov,; M. A. Petrukhina,; S. H. Strauss,; O. V. Boltalina. C20H4 (C4F8) 3: A Fluorine-Containing Annulated Corannulene that Is a Better Electron Acceptor Than C60. *Angew. Chem. Int. Ed*. **2013**, *52*, 7505–7508

26. A. Haupt, R. Walter, B. Loll, D. Lentz. Tetracyanocorannulene–an Easily Accessible and Strongly Electron-Deficient Compound *Eur. J. Org. Chem*. **2018**, *2018*, 6338–6342

27. Barát, V., Budanovic, M., Tam, S. M., Huh, J., Webster, R. D., Stuparu, M. C. Corannulene-Based Electron Acceptors: Combining Modular and Practical Synthesis with Electron Affinity and Solubility. *Eur. J. Chem.* **2020**, *26*(15), 3231-3235.

Chapter 3.

Experimental materials and methods

3.1. General materials and apparatus used.

3.2. Electrochemical setups in analysing BPA current amplification.

3.3. Coating of GCE surface.

3.4. In-situ electrochemical/UV-vis setup for corannulene analysis and General procedures for EPR analysis.

3.1 General materials and apparatus used.

All chemicals and reagents were of analytical grade and used as received. Multi-walled carbon nanotubes with carboxylic acid functionalization (>95%, 0.471-0.51 wt% -COOH, 50-80 nm diameter and 10-20 μm length) were obtained from Nanostructured and Amorphous Materials Inc. in Texas, USA and used as received. Iron (II, III) oxide nanopowder (>97%, 50-100 nm) was purchased from Sigma Aldrich and used directly as received. Solvents such as *N,N*-dimethyformamide (DMF) and acetonitrile (CH_3CN) were purchased from Alfa Aesar and Fisher Chemical. Ultrapure water used were obtained from an ELGA Purelab Option-Q water purification system with a resistivity of not less than 18 MΩ cm at 25°C. Tetrabutylammonium hexafluorophosphate (n-Bu_4NPF_6) was used as the supporting electrolyte for electrochemical experiments and was prepared by reacting equimolar amounts of aqueous solutions of n-Bu_4NOH (40%, Alfa Aesar) and HPF_6 (65%, Fluka), washing the white precipitate with ultrapure water until the pH was neutral, recrystallizing three times from hot analytical grade ethanol and drying under vacuum at 413 K for 6 hours.

Scanning electron microscopy (SEM) measurements were carried out by JEOL JSM-7600F Schottky Field Emission Scanning Electron Microscope at 5 kV of voltage acceleration. It was equipped with a canning Transmission Electron Microscopy detector for the acquisition of brightfield and darkfield images. Further processing was carried out with ImageJ software. Energy Dispersive X Ray (EDX) analysis measurements were carried out with the JSM-7600F Schottky Field Emission Scanning Electron Microscope at 15 kV of voltage acceleration. For EDX analysis, the voltage acceleration selected was twice of the highest peak energy expected. For the analysis of iron elements in MWCNTs-COOH/ Fe_3O_4 and MWCNTs-COOH/ Fe_3O_4/ PVP samples, a 15kV voltage acceleration was selected as iron has the highest peak energy of

6.398 kV. Oxford Instruments Aztec Version 3.3, copyright 2010- 2016, processing analysis software was used.

3.2. Electrochemical setups in analysing BPA current amplification

A three-electrode cell was used in a Faraday cage to minimize any external electromagnetic interference, and electrochemical procedures were carried out using a Metrohm Autolab PGSTAT302N potentiostat. The counter electrode consisted of a platinum wire and the reference electrode was a silver wire inside a Teflon sleeve containing 0.5 M *n*-Bu_4NPF_6 in CH_3CN separated from the test solution with a porous glass membrane. The working electrode was a 3 mm diameter GC electrode from Metrohm that was modified by dropcasting with the nanomaterials. Test solutions used CH_3CN as the solvent to allow for solubility of the analytes at 1 mM concentration and contained 0.1 M *n*-Bu_4NPF_6 as the supporting electrolyte. The bare GC electrode was firstly immersed into the analyte solution with the counter and reference electrode and subsequently swapped with the modified electrode coatings for comparison. All experiments were conducted at room temperature (22 ± 2ºC) with freshly prepared modified MWCNT-Fe_3O_4/GCE for single use for each voltametric experiment.

3.3. Coating of GCE surface.

62.5 mg of MWCNTs and 62.5mg Fe_3O_4 nanoparticles were pre-weighed respectively to make up a suspension in 0.50 wt% present in 25.0 ml of DMF. The MWCNT-Fe_3O_4 suspension were then ultrasonicated for 15 minutes at room temperature with the use of an ultrasonicator (Elmasonic E30H) at a frequency of 37 kHz to ensure mixing and dispersion of the nanoparticles. A bare glassy carbon (GC) electrode (3 mm diameter surface) was polished using 0.3 μm grit alumina oxide powder on a polishing cloth and rinsed thoroughly with ultrapure water and dried with lint-free paper before dropcasting a 5μL aliquot of the MWCNT-Fe_3O_4 suspension onto the surface using a micropipette. The GC electrode was left in air for the solvent to evaporate before using for electrochemical analysis.

To incorporate the addition of PVP surfactant, an aliquot was removed from the uniformly sonicated MWCNTs-COOH/Fe_3O_4 nanocomposite suspension and centrifuged at 12,000 rpm for 30 min using a Thermo Fisher Scientific Sorvall ST8R centrifuge. The pellet collected after centrifugation was dried overnight at 60 °C to obtain the MWCNTs-COOH/Fe_3O_4 solid material. Next, 0.05 g of this solid was introduced into a solution of 0.1 g PVP dissolved in 10 mL of deionized water:ethanol solution (1:1 v/v). The resulting MWCNTs-COOH/Fe_3O_4/PVP nanocomposite suspension was stirred magnetically at room temperature overnight. This suspension was then subjected to repeated water washing cycles using centrifugation until the supernatant reached neutral pH. The final pellet was dried under vacuum at room temperature followed by overnight drying in an oven at 60 °C. The dried MWCNTs-COOH/Fe_3O_4/PVP nanocomposite (0.5 g) was dispersed in 25 mL of DMF to yield a 2% w/v suspension.

3.4. In-situ electrochemical/UV-vis setup for corannulene analysis and General procedures for EPR analysis.

All voltametric measurements were performed using a Metrohm Autolab PGSTAT302N potentiostat in a three-electrode cell. A 1 mm diameter planar glassy carbon disk (GC, Cypress Systems) was used as a working electrode in conjunction with a platinum wire counter electrode (Metrohm) and an Ag/Ag^+ reference electrode. The analytical solutions were comprised of 0.1 M tetra-n-butylammonium hexafluorophosphate (n-Bu_4NPF_6) in dichloromethane (DCM), in which the corannulene-based compounds were fully dissolved. n-Bu_4NPF_6 was synthesized through a standard procedure according to the literature and used as the supporting electrolyte[24].

All voltametric experiments were conducted under an argon atmosphere, at room temperature (22 ± 2 ºC) in a Faraday cage. Prior to each scan, the working electrode was cleaned by polishing with an alumina oxide (grain size 0.3 μm) slurry on a Buehler Ultra-pad polishing cloth, rinsing with acetone, and then dried with a lint free tissue. In accordance with IUPAC recommendations, the absolute potentials were calibrated using ferrocene (Fc) as an internal reference, which was added to the test solution at the end of the measurements.

UV-vis spectra were collected on a Perkin-Elmer Lambda 750 spectrophotometer during the electrolysis of compounds **1** and **2** in an optically semi-transparent thin layer electrochemical (OSTLE) cell (pathlength = 0.05 cm) using a Pt mesh working electrode. The sample to be placed in the OSTLE cell was first deoxygenated by purging with Ar gas and the OSTLE cell was placed in a Schlenk tube and then filled with the deoxygenated analyte solution with a syringe. An Ag electrode was assembled using a thin piece of silver wire in a glass frit filled with 3 M *n*-Bu_4NPF_6 solution in DCM.

EPR spectra were obtained EPR spectra were obtained from electrolyzed solutions of corannulene **1** and **2** in DCM at the first reduction potential at 22 (±2) °C in an electrolysis cell.

The electrolysed solution was then transferred under nitrogen to a quartz flat cell, and recordingcontinuous wave X-band spectra with a Bruker ELEXSYS E500 EPRspectrometer.

Chapter 4. Electrochemical Current Amplification of Bisphenol A in the presence of magnetite nanoparticle composites

4.1 Introduction

4.2 Experimental Outline

4.3 Results and discussion

4.4 Characterization using SEM and EDX

4.5 Summary

4.6 References

4.1 Introduction

Previous chapters have mentioned that Bisphenol A (BPA) is one of the most pervasive and extensively manufactured compounds in the world and could potentially pose severe threats to the health of populations. Among different detection techniques reviewed, electrochemistry was highlighted as one the most effective ways for detecting trace BPA due to its capability for real-time analysis, streamlined workflows, and cost-effectiveness. However, as mentioned in chapter 2, this research field is defined by a series of trade-offs between priorities such as sensitivity and portability, and there are currently many other effective methods in use in BPA detection.

For example, in terms of pure sensitivity, fluorescence methods theoretically can provide the highest sensitivity. Under ideal, controlled laboratory conditions such as confocal microscopy, fluorescence can be used to detect and image single molecules[1]. As portable sensors don't operate at this extreme limit, this principle gives most portable sensors a very low theoretical detection limit. However, in the case of BPA fluorescence methods are greatly compromised as BPA is fundamentally non-fluorescent and requires probing.

Also, fluorescence faces a lot of optical interferences[2] when using real samples as real samples can contain many things that are naturally fluorescent (e.g., proteins, humic acid in soil, other phenols). Even clear water to the naked eye have to be pretreated for filtration to remove any particulate that could potentially scatters light, when performing experiments at ultra-low concentrations.

Calorimetry can be the most simple can cheap method in the detection of BPA as it makes use of physical changes such as colour of the analyte upon exposing to test kits containing chemically active enzymes[3] or nanoparticles[4]. However calorimetry often does not possess high sensitivity as visual color changes are often too subtle to be detected by the human eye or

camera/smartphone devices. There is a minimum concentration required to produce a visible color change that the eye or a basic camera can distinguish from the background.

Electrochemical methods are more balanced in terms of sensitivity and portability when detecting BPA and that is the reason the project aims to make use of electrochemistry to improve on the signal amplification resulting from BPA oxidation. The ability to tune the electrode surface for modification to achieve different modes for signal amplification makes this method a more balanced approach than other portable methods.

This chapter demonstrates that modifying a glassy carbon electrode (GCE) surface with a nanocomposite comprising magnetite nanoparticles (FeNPs) and functionalized multi-walled carbon nanotubes (f-MWCNTs), stabilized using polyvinylpyrrolidone (PVP) surfactant, yields a substantial amplification of the current signal response for BPA when performing cyclic voltammetry (CV) experiments.

4.2 Experimental Outline

2% w/v suspension comprising 0.25g of Functionalised multi-walled carbon nanotubes and 0.25g of magnetite nanoparticles (FeNPs) in 25ml of *N,N*-Dimethylformamide (DMF) were dropcasted onto glassy carbon electrode (GCE) surface evenly. The DMF were allowed to dry from evaporation to make leave the composite onto the electrode surface.

The use of f-MWCNT were used to support the FeNPs on the glassy carbon electrode (GCE) surface effectively. It was observed that FeNPs on their own were unable to be adhered effectively on the GCE surface using the drop casting procedure and detached via the effects of gravity when the electrode was immersed in solution. The introduction of f-MWCNT as an adhesive served as a connecting bridge between the FeNPs and the GCE surface. This was likely achieved through the electrostatic force of attraction between the functionalized MWCNTs and Fe3O4 nanoparticles The exact MWCNTs have -COOH functionalized groups that coordinate to the Fe2+/Fe3+ in the ionic structure:

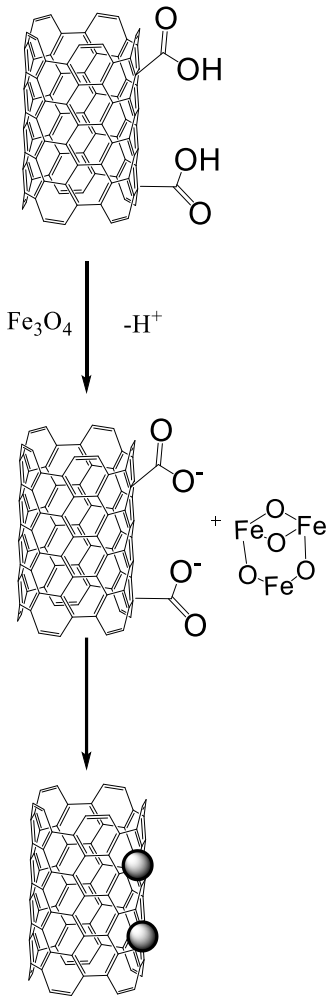

Figure 6. Illustration of the electrostatic forces of attraction between f-MWCNTs and FeNPs

The electrochemical behavior of iron nanoparticles (FeNPs) deposited onto the electrode surface was characterized using cyclic voltammetry (CV), as presented in **Figure 7**. This technique probed the redox processes accessible to the FeNPs, revealing their capacity to be both oxidized and reduced. This bifunctionality arises intrinsically from the presence of mixed-valence states within the nanoparticle structure, specifically Fe^{2+} and Fe^{3+} ions

(1) $Fe_3O_4 + 8H^+ + 2e^- \rightleftharpoons 3Fe^{2+} + 4H_2O$

(2) $2Fe_3O_4 + H_2O \rightleftharpoons 2Fe_2O_3 + 2H^+ + 2e^-$

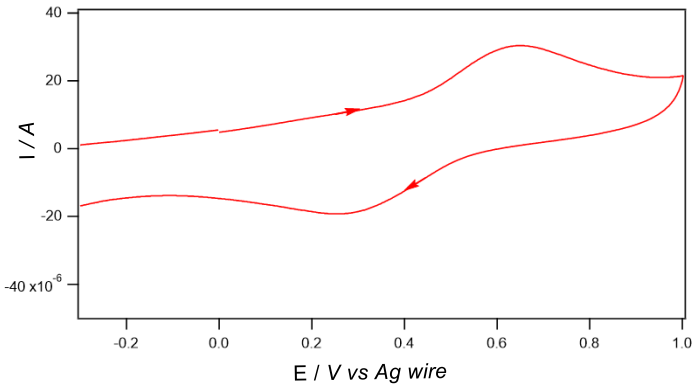

Figure 7. CV showing the oxidative process of FeNPs.

The underlying redox transitions governing the observed voltametric response are defined by Equations 1 and 2. Equation 1 describes the cathodic (reduction) process, where Equation 2 describes the anodic (oxidation) process. redox couple is fundamental to the FeNPs' demonstrated reducing and oxidizing capabilities, underpinning their potential for electrocatalytic functionalities.

4.3. Results and discussion

A significant practical limitation was observed during the CV analysis of the drop-cast FeNPs/f-MWCNT films. Despite exhibiting the characteristic redox processes, the FeNPs/f-MWCNT demonstrated poor adhesion to the bare electrode substrate. This instability manifested as visible detachment of the nanoparticle layer from the electrode surface immediately during initial scans due to gravity.

After investigation it was found that significant aggregation of iron nanoparticles (FeNPs) and functionalized multi-walled carbon nanotubes (f-MWCNTs) was observed on the glassy carbon electrode (GCE) surface which hinders the adhesiveness towards the GCE itself. This phenomenon is attributed to strong intermolecular attraction forces, primarily electrostatic interactions arising from the surface charges on the nanomaterials, compounded by π-π stacking tendencies of the f-MWCNTs. This aggregation resulted in a heterogeneous distribution of the FeNPs/f-MWCNT composite across the electrode surface. Causing the effective surface area exhibited substantial variability between replicate experiments. Due to the direct relationship between electroactive surface area and faradaic current in voltammetry, this heterogeneity manifested as significant inter-experimental variation in the measured peak currents. To mitigate aggregation and enhance dispersion stability, an anionic polyvinylpyrrolidone (PVP) surfactant was introduced. PVP adsorbs onto the nanoparticle and nanotube surfaces, providing steric stabilization through its polymeric chains and electrostatic repulsion via its anionic groups (**Figure 8**). This stabilization promotes a more uniform dispersion of the FeNP/f-MWCNT composite, leading to a consistent and reproducible electroactive surface area on the modified GCE.

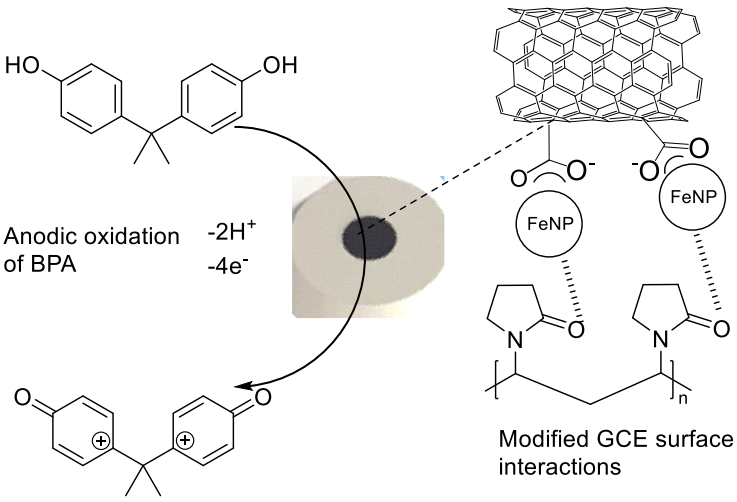

Figure 8. Interactions between the PVP surfactant and modified GCE surface for stability

In order to justify the current amplification capability from the composite system, a comparison between the modified surfaces were carried out. It turned out that modifications with either MWCNTs or Fe_3O_4 nanoparticles individually enhanced the electrochemical response. Coating the glassy carbon electrode (GCE) with multi-walled carbon nanotubes (MWCNTs) resulted in an increase of the oxidation peak current (i_p^{ox}) to 98 µA [**Figure 9(*a*)**]. Similarly, modification with Fe_3O_4 nanoparticles increased the i_p^{ox} to 200 µA [**Figure 9(*c*)**]. These results demonstrate that both materials independently contribute to signal amplification.

A synergistic enhancement was achieved with a composite MWCNT/Fe_3O_4 modification. When Fe_3O_4 nanoparticles were combined with MWCNTs on the GCE surface, the nanoparticles remained effectively immobilized. This stable composite modification yielded a significantly higher i_p^{ox} of 590 µA [**Figure 9(*d*)**]. This current represents an approximately 13-fold amplification compared to the oxidation peak signal obtained at the bare GCE.

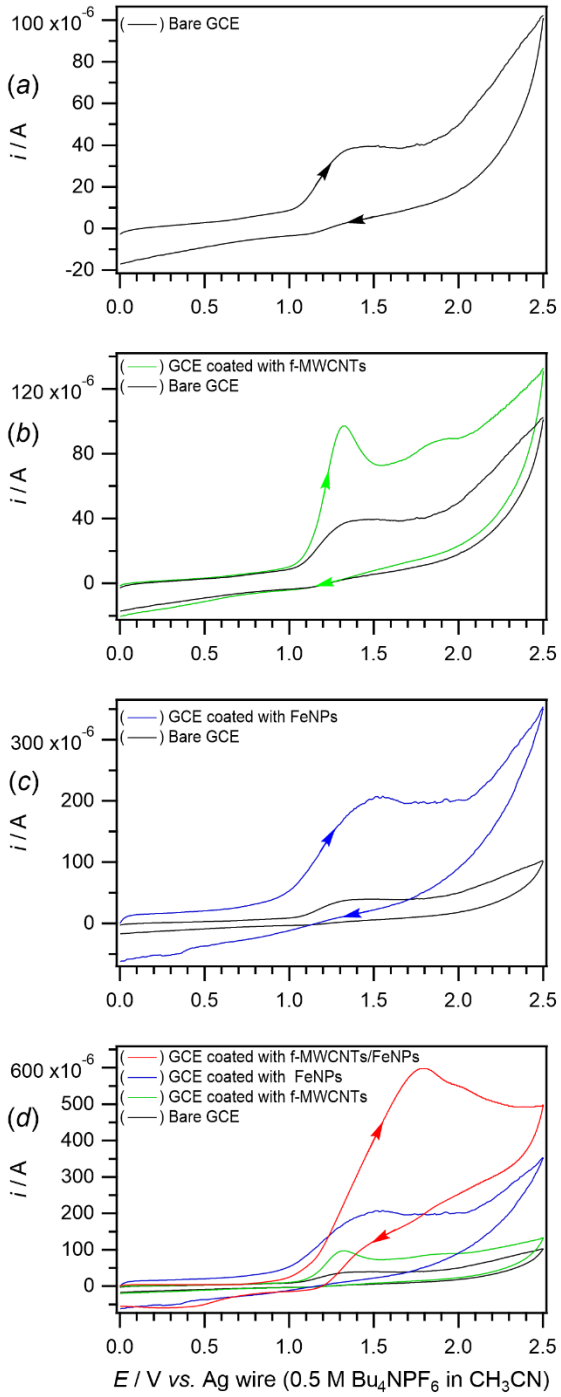

Figure 9. Cyclic voltammograms of 1 mM BPA in CH_3CN containing 0.1 M *n*-Bu_4NPF_6 at a scan rate of 0.1 V s^{-1}. (*a*) bare GCE, (*b*) comparison between bare GCE *vs.* GCE coated with MWCNTs, (*c*) comparison between bare GCE *vs.* GCE coated with Fe_3O_4 nanoparticles only, and (*d*) comparison between bare GCE *vs.* coatings in *b* and *c* and at a GCE coated with both MWCNTs and Fe_3O_4 nanoparticles.

The CV in **Figure 9(*a*)** shows an oxidation peak (E_p^{ox}) of BPA at approximately 1.4 – 1.6 V *vs.* Ag wire with an oxidative peak current (i_p^{ox}) of ~40 µA with the use of a bare GCE. When the GCE was coated with f-MWCNTs [**Figure 9(*b*)**] or FeNPs [**Figure 9(*c*)**], the i_p^{ox} increased to 98 µA and 200 µA respectively, indicating that both f-MWCNTs and FeNPs can lead to signal enhancements by themselves. However, it was observed that some of the black FeNPs fell off the GCE surface as soon as it was immersed into the analyte solution. With the introduction of f-MWCNTs combined together with FeNPs, it was observed that the FeNPs remained attached to the electrode, and the i_p^{ox}-value was further enhanced significantly to 590 µA [**Figure 9(*d*)**], an approximately 13-fold amplification over the bare GCE oxidation peak signal.

Experiments were also conducted using non-functionalized multiwalled carbon nanotubes (MWCNTs) combined with the FeNPs and it was found that there was a large difference in peak current for the electrode coated with MWCNTs/FeNPs compared to the electrode coated with f-MWCNTs/FeNPs. The MWCNTs/FeNPs coated electrode showed significantly lower peak currents than the f-MWCNTs/FeNPs coated electrode, implying that the COOH-group does play a role in the overall current enhancement. As shown in **Figure 8**, it is proposed that the -COOH groups promote interactions between the f-MWCNTs and the FeNPs. The H^+ released during the initial oxidation process may be available to reprotonate the oxidized phenol when it undergoes reduction through interactions with Fe^{2+} in the FeNPs as illustrated in **Figure 10**, or the -COOH groups may also provide a source of protons. For this study, all experiments were conducted in CH_3CN because of the low solubility of the phenols in aqueous systems, thus pH-dependent studies were not undertaken. Nevertheless, trace water itself in acetonitrile may also be able to provide protons for the reduction reaction of BPA^{2+} back to BPA or for reactions with the FeNPs (eqs. 1 and 2).

It is important to note that the system depicted in **Figure 10** does not represent a true catalytic cycle in the sense that The FeNPs are not regenerated or unchanged; they are consumed through oxidation (Fe^{2+} to Fe^{3+} conversion) during the reduction of the BPA intermediates. However, under typical voltammetric conditions (characterized by short experimental timescales and the limited flux of analyte reacting with the nanoparticle surface), the depletion of active FeNPs is negligible and does not preclude the observation of significant signal enhancement. This is largely due to the fast experimental sweep time in CV (less than a minute). Which means the actual time with sufficient energy (E/V) for redox reaction to happen is even shorter. The FeNPs composite has a huge reservoir of active catalytic sites compared to the number of BPA molecules arriving at the surface during a single scan and the amount of FeNPs consumed by reducing BPA^{2+} is a tiny fraction (<1%) of the total available. Therefore, no significant depletion is observed within the duration of a single measurement.

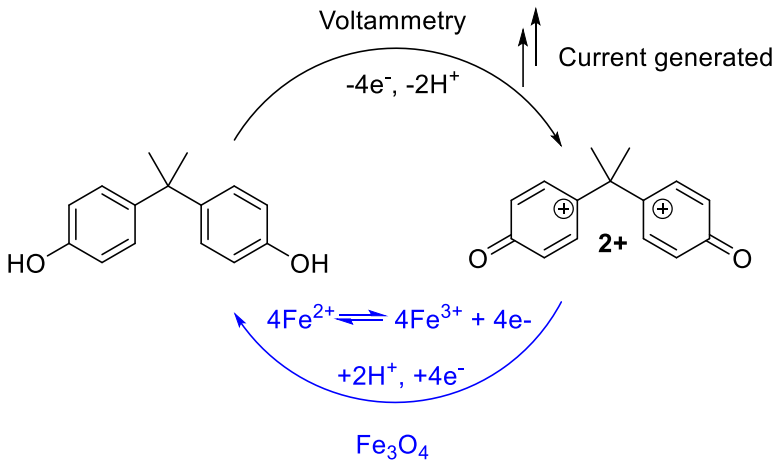

Figure 10. Mechanism of catalytic recycling of BPA through the constant reduction of FeNPs.

The mechanism for the loss of FeNPs lies in the dissolution of labile Fe^{3+} ions arising from oxidation of Fe^{2+}, when acting as a reducing agent to reduce BPA intermediates. Unlike solid

FeNPs, labile Fe^{3+}ion has a high charge density and is a strong Lewis acid. In the reaction environment with water present, it has a very strong tendency to form stable, soluble complexes with the water molecules. The reaction is thermodynamically favorable, especially if the local environment is slightly acidic which is true in this case as the reaction is coupled with production of H^+. With the presence of COOH group in f-MWCNT, the surface environment of the electrode is also slightly acidic.

The Fe^{3+} ion that dissolves is not from the core of the nanoparticle, it's specifically from the surface, and critically, from the interface where the FeNP is bonded to the f-MWCNT. Therefore although the loss of active sites can occur due to surface fouling from Fe^{3+} dissolution, the overall network does not fully break down for single event use.

The addition of PVP surfactant enhanced electrode performance through improved conductivity and stability due to aggregation prevention. The inclusion of PVP reduces particle agglomeration within the nanocomposite, facilitating BPA diffusion to the working electrode's active sites and effectively increasing its electroactive surface area. Furthermore, PVP contributes to enhanced nanocomposite conductivity during electrochemical processes. This conductivity increase is proposed to arise from ion-dipole interactions between the cationic oxidized BPA intermediates and the electronegative oxygen atoms within the PVP polymer chains, as depicted in **Figure 8**. This interaction brings the oxidized BPA species into closer proximity with the FeNPs/f-MWCNTs nanocomposite interface, enabling the catalytic properties of the FeNPs. Consequently, the FeNPs/f-MWCNTs/PVP modified working electrode exhibited the highest current amplification (i_p^{ox} > 1000 μA), illustrated by the red trace in **Figure 11**, demonstrating superior oxidative peak current compared to other coatings.

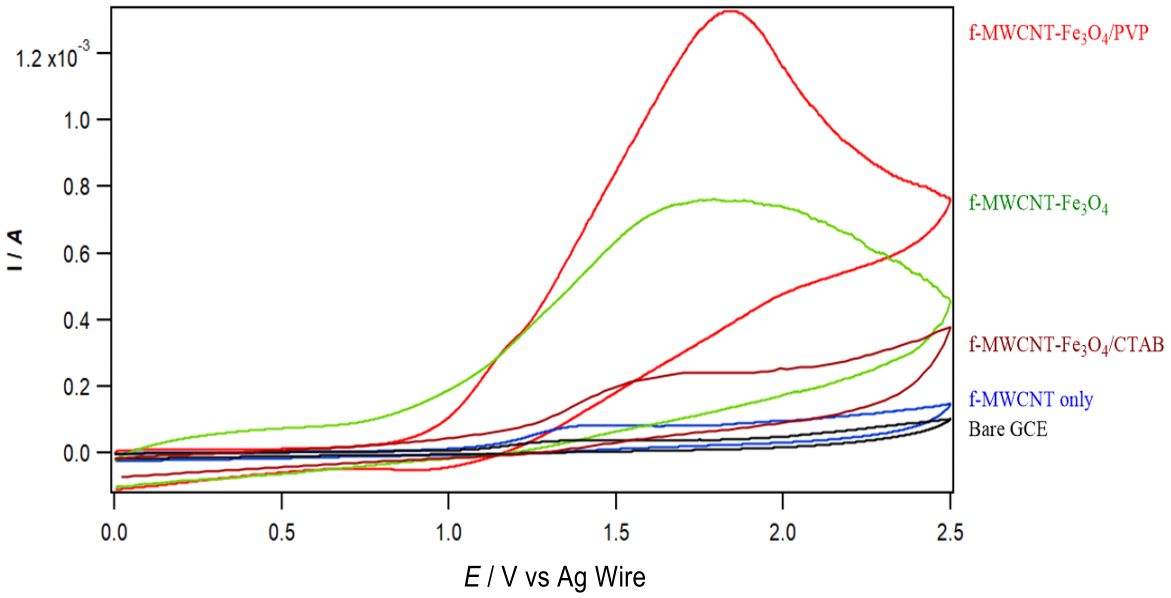

Figure 11. Cyclic voltammograms of 1 mM BPA in CH_3CN containing 0.1 M *n*-Bu_4NPF_6 at a scan rate of 0.1 V s^{-1} at a GCE drop cast with various composite materials including neutral and cationic surfactants.

In contrast, cationic surfactants like CTAB impair catalytic performance. Compared to the anionic PVP, the cationic surfactant cetyltrimethylammonium bromide (CTAB) failed to maintain high current amplification when incorporated into the FeNPs/f-MWCNTs composite. Drop-casting the GCE with the FeNPs/f-MWCNTs/CTAB composite resulted in decreased BPA oxidation current (brown trace, **Figure 11**). Specifically, while the FeNPs/f-MWCNT composite without CTAB yielded an i_p^{ox} of ~500 µA, the addition of CTAB significantly reduced the current to ~170 µA. This i_p^{ox} value is comparable to that observed with MWCNTs-COOH alone (170 µA), indicating that CTAB negates the catalytic enhancement provided by the FeNPs nanoparticles.

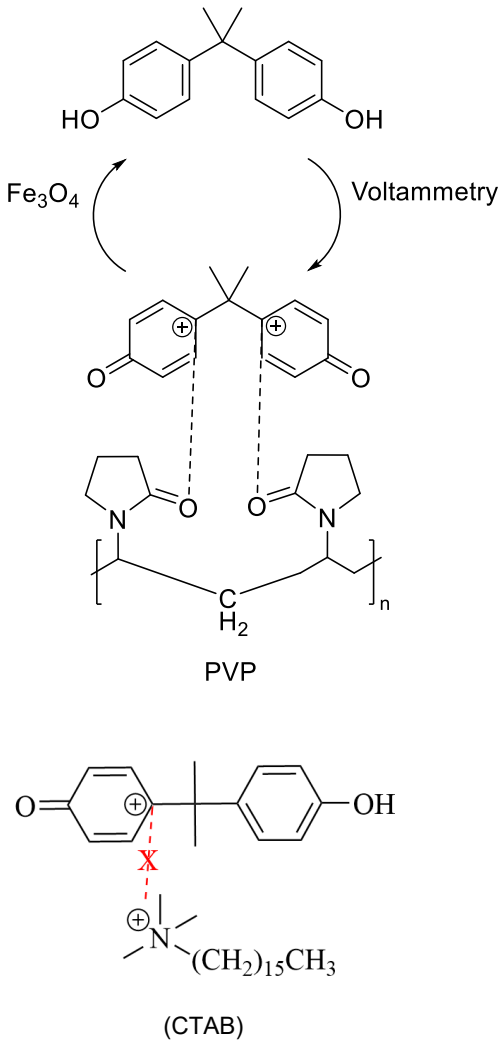

Figure 12. Comparison between the mode of interaction of BPA with neutral (PVP) and cationic (CTAB) surfactants.

The detrimental effect of CTAB is attributed to electrostatic repulsion. The performance failure of the FeNPs/f-MWCNTs/CTAB system likely results from electrostatic repulsion between the cationic CTAB surfactant and the cationic oxidized BPA species (**Figure 12)**. This repulsion prevents the close interaction of oxidized BPA with the nanocomposite interface necessary for the FeNPs to catalyze BPA regeneration, thereby diminishing the overall electrochemical response.

In general, each individual component in the xomposite system plays an important role in ensuring the overall effectiveness of current amplification:

FeNP – Directly contributes to the current amplification through analyte recycling. This creates a pseudo catalytic cycle: BPA(Neutral) → BPA(Oxidised) → BPA(Neutral), at the loss of dissolution of Fe^{3+} ions. The same amount of BPA molecules in diffusion layer is effectively measured multiple times in a single scan, leading to a repeated, and amplified current signal. This is a heterogeneous reaction happening directly on the electrode surface. By introducing FeNPs to the electrode surface, the effective surface area of the electrode also increases, which can also lead to small enhancements in current signals.

f-MWCNTs - The f-MWCNTs do not directly participate in the analyte recycling but are essential for making it possible and more efficient. The -COOH groups on the f-MWCNTs are negatively charged and able to form strong electrostatic force with the positively charged Fe^{2+}/Fe^{3+} ions on the FeNP surface. Simultaneously, the f-MWCNTs physically anchor to the surface of the Glassy Carbon Electrode (GCE), acting as a supporting bridge scaffold allowing for the immobilization of a much larger number of FeNPs, thereby multiplying the number of available sites for the catalytic recycling reaction.

PVP – The PVP surfactant ensures consistency to maximize the performance of the whole system. The very strong electrostatic attraction between FeNPs and f-MWCNTs may cause them to aggregate together and creates an uneven, non-uniform film on the electrode. In order to prevent this, PVP surfactant's long polymer chains are able to create a steric hindrance, physically preventing the particles from getting too close and aggregating. On top of that, this also ensures they form a uniform, thin film across the entire GCE surface, leading to more reproducible peak currents, which is essential for accurate quantitative analysis.

4.4 Characterization using SEM and EDX

The difference in degree of aggregation was supported by the characterization using Scanning Electron Microscopy (SEM):

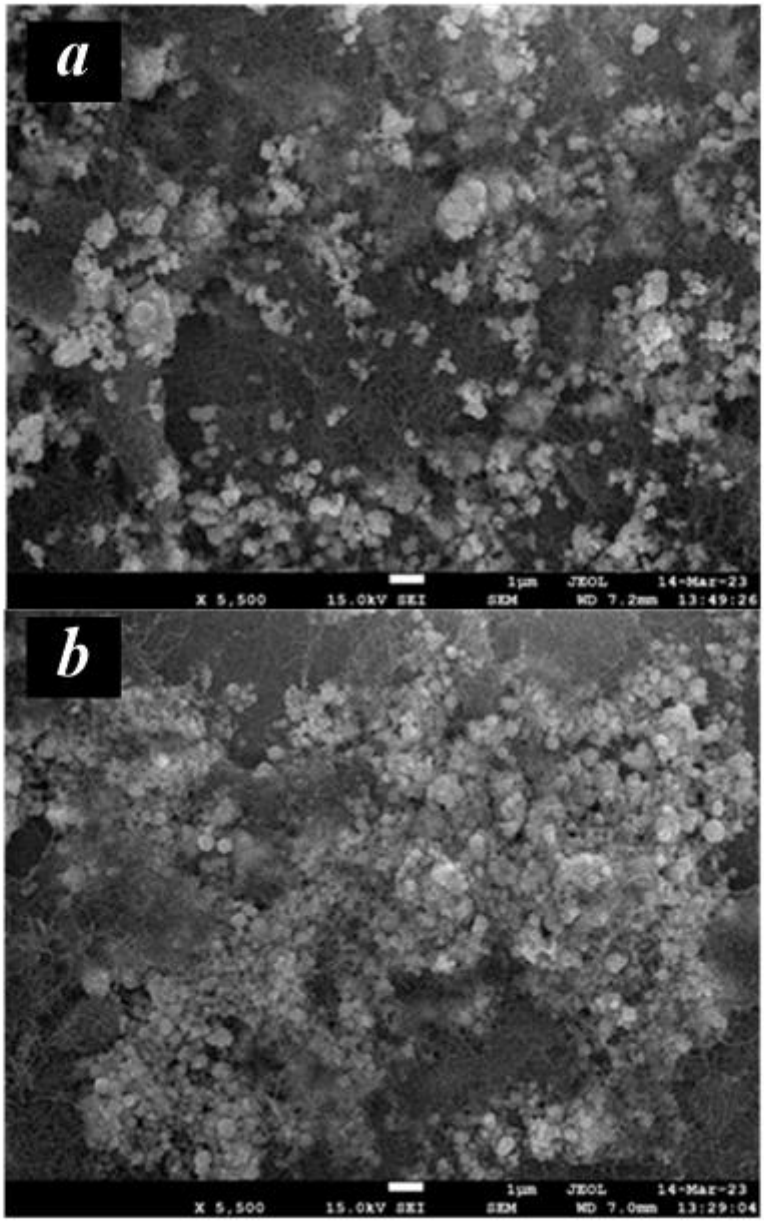

Figure 13. Comparison of residence per unit area of GCE surface covered by FeNP/f-MWCNT composite at 1 um resolution. (*a*) without PVP surfactant (*b*) with PVP surfactant.

Figure 13 demonstrates that PVP modification significantly reduces nanocomposite agglomeration and particle size. Prior to PVP functionalization, the f-MWCNTs component exhibited an average size of 63 ± 13 nm [**Figure 13 (*a*)**] Following PVP surfactant modification, this average size decreased substantially to 37 ± 8 nm [**Figure 13 (*b*)**]. Similarly, the average particle size of the Fe_3O_4 component within the nanocomposite decreased from 246 ± 90 nm to 126 ± 40 nm. This reduction in particle dimensions directly correlates with diminished nanoparticle agglomeration, as facilitated by the PVP surfactant.

Reduced agglomeration enhances porosity and electrode coverage. The observed decrease in particle size and agglomeration state suggests the formation of a more porous nanostructure upon PVP incorporation. This shows that the FeNPs/f-MWCNTs/PVP composite [**Figure 13**(***b***)] achieved more uniform coverage on the electrode surface compared to the unmodified FeNP/f-MWCNTs nanocomposites [**Figure 13 (*a*)**]. Both composites exhibit clustered structures, indicating effective interfacial binding between the f-MWCNT and Fe_3O_4 nanoparticles.

It is thus believed that the increased porosity and effective surface area promote greater analyte diffusion to active sites, aligning with the previously proposed role of PVP in facilitating analyte access. Furthermore, the maintained effective binding between the MWCNTs-COOH and Fe_3O_4 nanoparticles is crucial for optimizing electrical conductivity and promoting catalytic interactions at the nanocomposite interface. These synergistic morphological improvements of reduced aggregation, enhanced porosity, and preserved catalytic interfaces contribute directly to the superior electrochemical performance observed with the PVP-modified electrode.

Energy-dispersive X-ray spectroscopy (EDX) also supports the improvement of the electrochemical performance of the FeNPs/f-MWCNTs/PVP modified working electrode. EDX mapping analysis was performed on the modified GCE surface functionalized with the nanocomposite (**Figure 14**) and confirmed the homogeneous elemental distribution and conductive pathways within the modified electrode. This technique spatially resolved the elemental composition, revealing a uniform distribution of iron (Fe) across the surface, originating from the Fe_3O_4 nanoparticles (FeNPs). Simultaneously, carbon (C) from both the functionalized multi-walled carbon nanotubes (f-MWCNTs) and the surfactant was also evenly distributed. Fe distribution directly correlates to accessible catalytic sites and uniform dispersion shows minimal agglomeration, ensuring a high density of exposed Fe_3O_4 nanoparticles available for catalytic reactions.

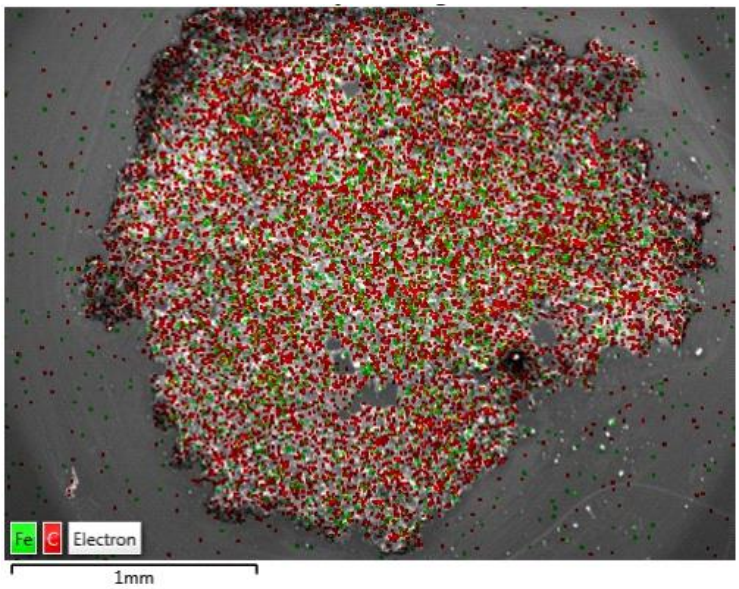

Figure 14. EDX image illustrating the elemental and free electron distribution of the composite layer on modified GCE surface

Energy-dispersive X-ray diffraction spectroscopy (EDX) was also carried out on the modified GCE surface (**Figure 14**). Elemental distribution of iron (from FeNPs) and carbon (from f-MWCNTs and surfactant) showed an even distribution of FeNPs on the surface of the GCE.

The white areas represent the backscattered electron (BSE) image overlay showing compositional and topographical differences in the spectrum. Additional SEM images and EDX characterization is provided in Figures S4 – S6 in the Supplementary Information section, which include elemental compositions taken from different portions of the composite electrodes. TEM images of the f-MWCNTs/FeNPs composite indicated an average size of the FeNPs of 107 nm, while for the f-MWCNTs/FeNPs/PVP composite the average size was 91 nm. The difference is not considered significant and likely due to small sample variations (Figures S9 and S10 in the Supplementary Information section). The difference between the TEM results and SEM results is due to the TEM data being able to differentiate each individual FeNP, while the SEM results detected that aggregated FeNPs as essentially one particle.

The homogeneous distribution of catalytic Fe_3O_4 sites and the confirmed pervasive electron mobility are fundamental prerequisites for high electrode efficiency. The uniform Fe dispersion maximizes the electroactive surface area for analyte interaction and catalysis, while the interconnected conductive network ensures rapid charge transfer during redox processes. This synergy directly supports the robust redox activity by enabling efficient electron flow from the catalytic sites (Fe_3O_4) through the conductive backbone (f-MWCNTs) to the electrode substrate (GCE), minimizing resistive losses and facilitating fast reaction kinetics.

4.5 Summary

Pronounced oxidative peak current amplification and selectivity for BPA were achieved with the PVP-modified nanocomposite electrode. The fMWCNTs-COOH/Fe_3O_4/PVP nanocomposite coating on the GCE delivers exceptional BPA current amplification based on the following properties:

1. Enhanced morphology and accessibility: PVP surfactant critically reduces nanoparticle agglomeration, as evidenced by the significant decrease in composite and Fe_3O_4 particle sizes observed via SEM. Evident from 63±13 nm to 37±8 nm and 246±90 nm to 126±40 nm, respectively. This reduction in agglomeration increases porosity and creates a more uniform electrode coverage, significantly expanding the electroactive surface area and facilitating improved BPA diffusion to active sites.

2. Effective electron transfer: Fe_3O_4 nanoparticles provide essential catalytic activity, enabling the hypothesized BPA recycling mechanism. EDX mapping confirmed the homogeneous distribution of Fe substrate which indicates well-dispersed catalytic sites, demonstrating the establishment of highly conductive networks through contact between the fMWCNTs-COOH and Fe_3O_4. This ensures rapid electron transfer from catalytic sites to the electrode substrate.

3. Synergistic amplification: The combined effect of increased surface area/porosity from PVP dispersion and favourable interfacial interactions culminates in the pronounced amplification of the BPA oxidation peak current (i_p^{ox} > 1000 μA), representing a substantial improvement over the bare GCE and other composite formulations.

In conclusion, the fMWCNTs-COOH/Fe_3O_4/PVP modified GCE can potentially function as a high-performance sensor for BPA, leveraging synergistic nanomaterial properties, optimized interfacial chemistry, and catalytic recycling to achieve significant signal amplification.

4.6 References

1. W. E. Moerner,; D. P. Fromm. Methods of single-molecule fluorescence spectroscopy and microscopy. *Rev. Sci. instrum*. **2003.** *74*(8), 3597-3619.

2. M. Dandin,; P. Abshire,; E. Smela. Optical filtering technologies for integrated fluorescence sensors. *Lab on a Chip*, **2007.** *7*(8), 955-977.

3. R. S. Alkasir,; A. Rossner,; S. Andreescu. Portable colorimetric paper-based biosensing device for the assessment of bisphenol A in indoor dust. *Enviro. Sci. Technol*. **2015.** *49*(16), 9889-9897.

4. E. H. Lee,; S. K. Lee,; M. J. Kim,; S. W. Lee. Simple and rapid detection of bisphenol A using a gold nanoparticle-based colorimetric aptasensor. *Food Chem.* **2019.** *287*, 205-213.

Chapter 5. Electrochemical characterization analysis of corannulene based compounds as electron acceptors - A collaboration project with Assoc. Prof. Mihaiela Stuparu

5.1 Introduction

5.2 Electrochemical behavior of 15 investigated corannulene compounds

5.3 Results and discussion

5.4 In situ UV-vis spectroscopy electrolysis analysis

5.5 Confirmation of radical species using EPR spectroscopy

5.6 Summary

5.7 References

5.1 Introduction

The primary goal in developing functionalised corannulene-based acceptors is to hope to replace current electron acceptors such as fullerenes like PCBM. Therefore, their electron-accepting capability is one of the most critical property to benchmark. Higher electron affinity indicates that a low-lying, stable LUMO is present. This energy difference between the LUMO of the acceptor and the HOMO of the donor provides the thermodynamic driving force for the electron to be accepted by the acceptor.

There are many methods such as Ultraviolet Photoelectron Spectroscopy[1] (UPS) or computational methods like DFT[2] which can estimate energy levels. Electrochemistry, particularly Cyclic Voltammetry (CV) and Square-Wave Voltammetry (SWV), has an advantage in terms of able to directly probe and observe the reductive process. Techniques like UPS or UV-vis which estimates the photoelectronic band gaps are indirect methods as they measure electron adsorption and not electron addition itself. Meanwhile, DFT is a computational prediction model which is highly reliant on the functional and basis set used. Experimental electrochemical data is more often needed to validate and calibrate these computations further.

In terms of using electrochemistry, the first reversible reduction potential ($E_{r1/2}$) can be measured and is able to show how effective an electron acceptor a new corannulene derivative is, allowing them to directly compete with the benchmark of PCBM. Simultaneously, the i_p^{ox}/i_p^{red} ratio is able to show if the molecule is robust enough to survive the harsh redox cycling in an operating device, which will be further elaborated in the later section using *in situ* electrochemical-UV-vis experiments.

This chapter investigates the electrochemical behavior of 15 substituted corannulene derivatives, whose structures are detailed in Table 2, primarily through measurement of the first reversible reduction potential. This potential, denoted as $E_{r1/2}$ is determined as the midpoint between the cathodic (E_p^{red}) and anodic (E_p^{ox}) peak potentials:

$$E_f^0 \approx E_{r1/2} = [(E_p^{red} + E_p^{ox})/2]$$

The ratio of oxidative to reductive peak currents (i_p^{ox}/i_p^{red}) obtained from CV also serves as an indicator of the chemical stability of the electrogenerated reduced species on the timescale of the voltammetric scan rate. For electrochemically reversible processes, a ratio (i_p^{ox}/i_p^{red}) ≥ 0.97 typically signifies complete stability of the reduced species during the experiment, whereas ratios falling below 0.97 suggest chemical reactivity or instability. Lower ratios generally imply greater reactivity.

Complementary to the CV assessment of electrochemical reversibility and the chemical stability of the electrogenerated reduced species, in-situ electrospectroscopic experiments, specifically UV-Vis spectroscopy coupled with controlled-potential electrolysis, is performed to probe the lifetime and spectroscopic signatures of the reduced species generated *in situ*, providing critical insights into the compounds' suitability as electron-accepting materials.

5.2 Electrochemical behavior of 15 investigated corannulene compounds

15 corannulenes with different substituted functional groups were studied using cyclic voltammetry and their respective structures are provided in **Table 2**. The effect of the substituted functional groups can be assessed based on measurements of the first reversible reduction potential or wave-wave potential ($E^{r}_{1/2}$), which approximates the formal potential (E^{0}_{f}).

Table 2. Structures of corannulene 1-15:

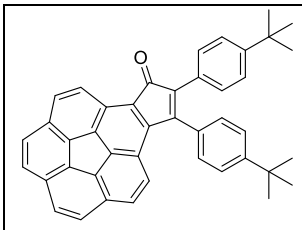 **1**	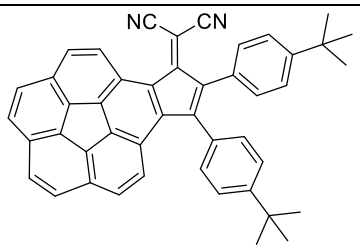 **2**	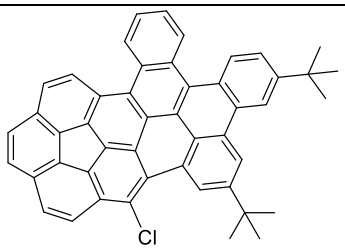 **3**
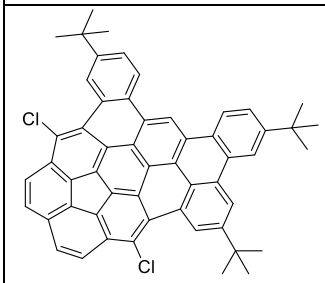 **4**	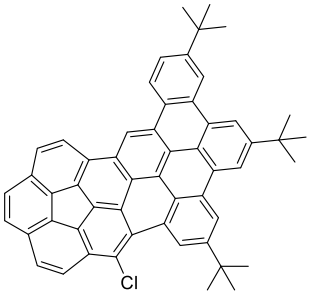 **5**	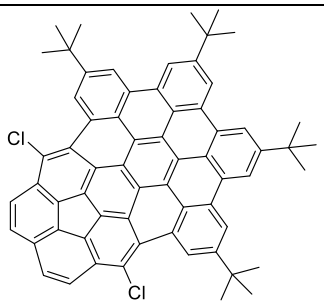 **6**
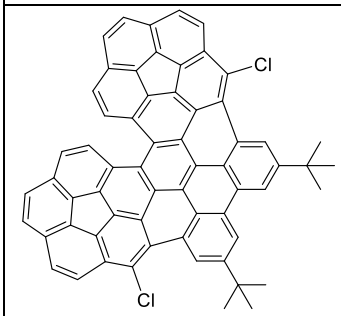	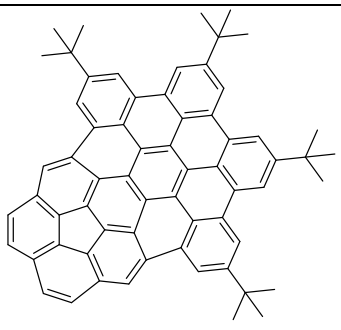	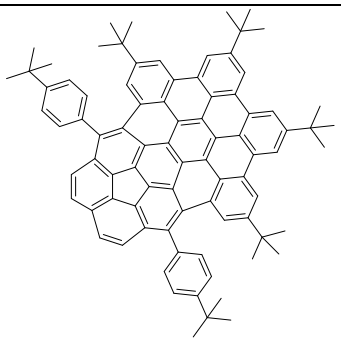

7	8	9
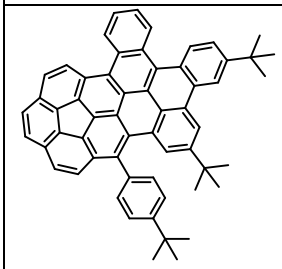 **10**	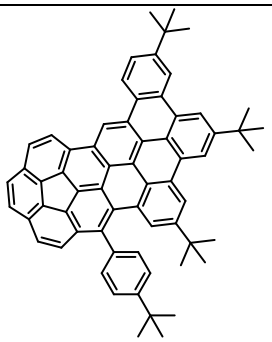 **11**	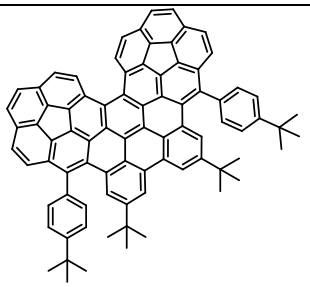 **12**
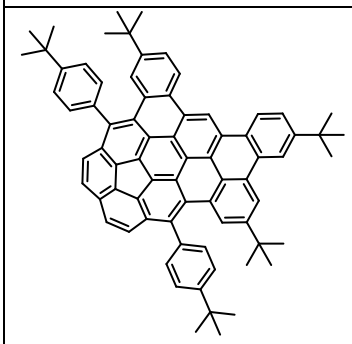 **13**	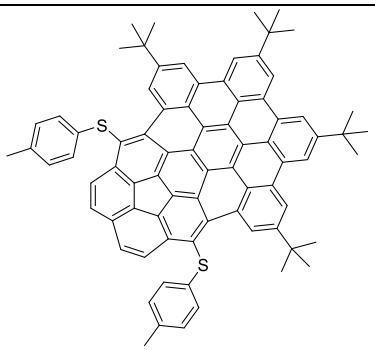 **14**	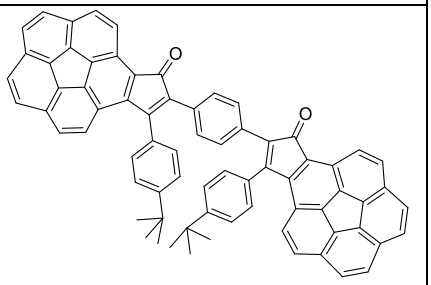 **15**

5.3 Results and Discussion

Cyclic voltammograms of the 15 corannulenes depicting their first reduction potential were shown in **Figure 15** below, based on increasing negativity of E_p^{red}

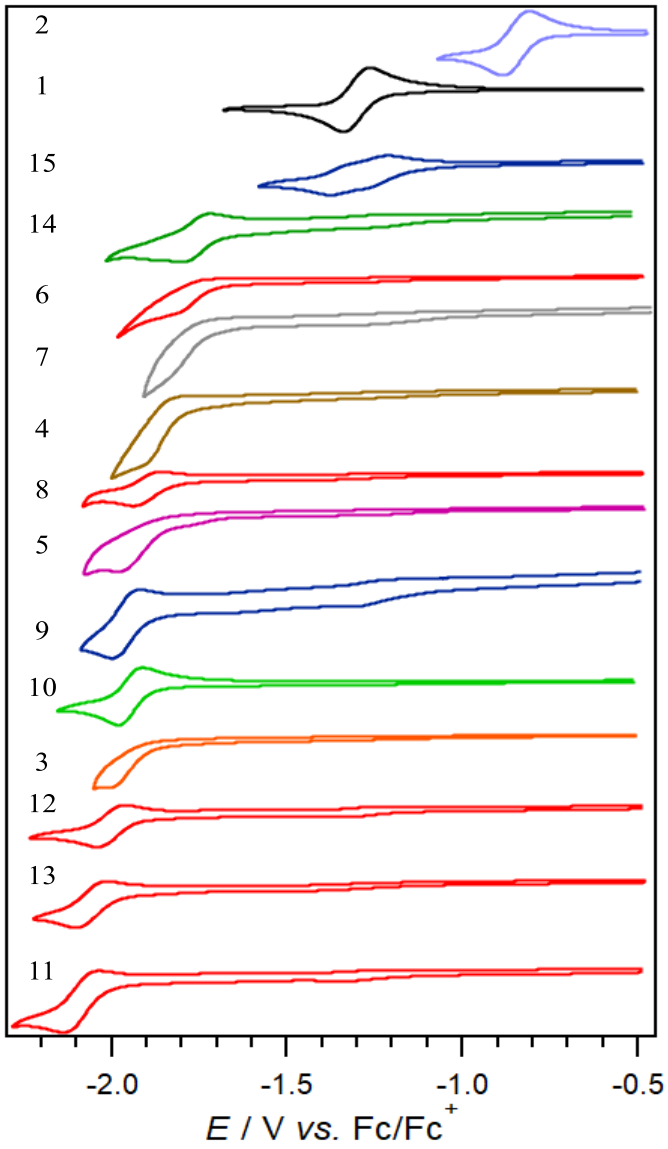

Figure 15. CV voltammogram of first reduction potential of the 15 corannulene-based compounds

For an electrochemically reversible process (fast electron transfer) the oxidative peak current (i_p^{ox}) to the reductive peak current (i_p^{red}) ratio (i_p^{ox}/i_p^{red}) measured by CV is an indication of the chemical stability of the reduced species at a defined voltammetric scan rate. i_p^{ox}/i_p^{red}-values ≥ 0.97 indicate that the reduced species is completely stable (does not decompose) on the timescale of the experiment, whereas $i_p^{ox}/i_p^{red} < 0.97$ indicate chemical reactivity of instability of the reduced species, with values further from unity implying greater reactivity. However, there are situations where i_p^{ox}/i_p^{red}-values ≈ 1 are obtained and the reduced species do undergo follow-up chemical reactions, such as for reversible dimerization reactions, where the follow up processes are themselves chemically reversible[21,22]. Similarly, $i_p^{ox}/i_p^{red} << 0.97$ can be obtained in situations where the reduced species are long-lived, but are in chemical equilibrium, thus may not appear to be able to be completely reduced back to the starting materials[21,22]. Nevertheless, the i_p^{ox}/i_p^{red}-ratios are often used as an approximate measure of lifetime of the reduced species, with values close to unity suggesting complete chemical stability of the timescale of the voltammetric scan. Table 3 provides the one-electron reduction potentials ($E^r_{1/2}$) measured by CV or SWV and the corresponding i_p^{ox}/i_p^{red}-ratios measured by CV at a scan rate of 0.1 V s^{-1}.

Table 3. E^0_f/V of the 15 corannulenes and their i_p^{ox}/i_p^{red}-value

Corannulene	E^0_f/ V vs. Fc/Fc^+	i_p^{ox}/i_p^{red}-value
1	-1.34	~1.0
2	-0.84	~1.0
3	-2.06	0
4	-1.91	0
5	-1.99	0
6	-1.76	0

7	-1.82	0
8	-1.94	~1.0
9	-1.97	~1.0
10	-2.05	~1.0
11	-2.10	~1.0
12	-1.93	0
13	-2.02	0
14	-1.76	~0.6
15	-1.25	~0.6

From the data in **Table 3**, it can be observed that all the corannulene compounds have their first reduction potential lowered to more positive potentials as compared to pristine corannulene (-2.31 V *vs.* Fc/Fc^{+}) due to the presence of electron withdrawing substituents such as Cl (**3-7**), arene (**8-13**), O (**1**, **15**), S (**14**) and CN (**2**). However, the corannulenes differ substantially in their i_p^{ox}/i_p^{red}-ratios, and, if it is assumed that the lifetime of the reduced states increases as the ratios approach unity, some conclusions can be made about the chemical stability of the radical anions. The corannulenes with chlorine substituents (**3-7)** are not long-lived after electrochemical reduction, most likely due to homolytic cleavage of the C-Cl bond which generates a stable and inert Cl^- ion, and a reactive corannulene neutral radical, which is a common result seen during the reduction of aromatic halides[23].

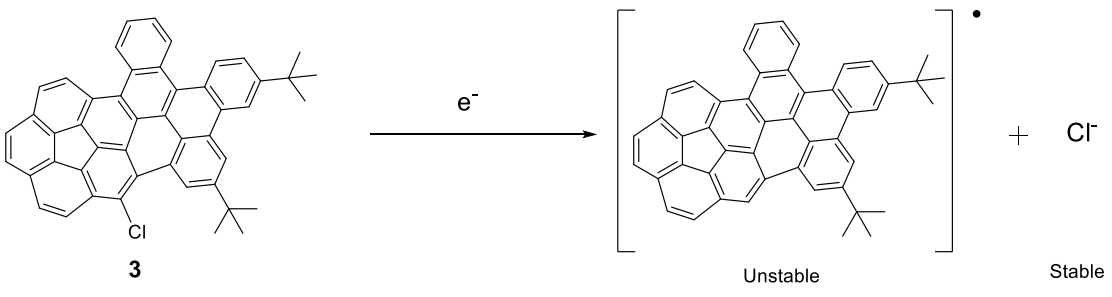

Figure 16. Illustration of first reduction of a chlorinated corannulene

Therefore, although the first reduction potential of the chlorinated **3-7** corannulenes are all lower and lie between -1.7 V ~ -2.1 V *vs.* Fc/Fc^+ as compared to pristine corannulene (-2.31 V *vs.* Fc/Fc^+), the relatively short lifetimes of their radical anions limit the electron storing capacity and practicality of the chlorinated substituted corannulene compounds for use as electron acceptors. This is also applicable to corannulenes **5** and **15**, where although their -S and -O substituents provide an enhanced first reduction potential, the chemical instability of the one-electron reduced states make them unsuitable as candidates as electron acceptors in electronic devices.

In contrast, it was observed that the corannulenes **8** – **13** with extended aromatic systems displayed i_p^{ox}/i_p^{red}-ratios close to unity implying high stability in their one-electron reduced states. All these compounds also displayed low E^0_f-values, partially due to the increased size of their aromatic structure, allowing extensive delocalization of the unpaired electron and thereby lowering the energy required to take in an additional electron. Out of these compounds, **12** contains two corannulene cores and displays the highest enhancement of the first reduction potential of -1.93 V *vs.* Fc/Fc^+, while **8** being the largest molecule with the most extensive overall aromatic system displays the second highest enhancement at -1.97 V vs. Fc/Fc^+ (**Figure 17**).

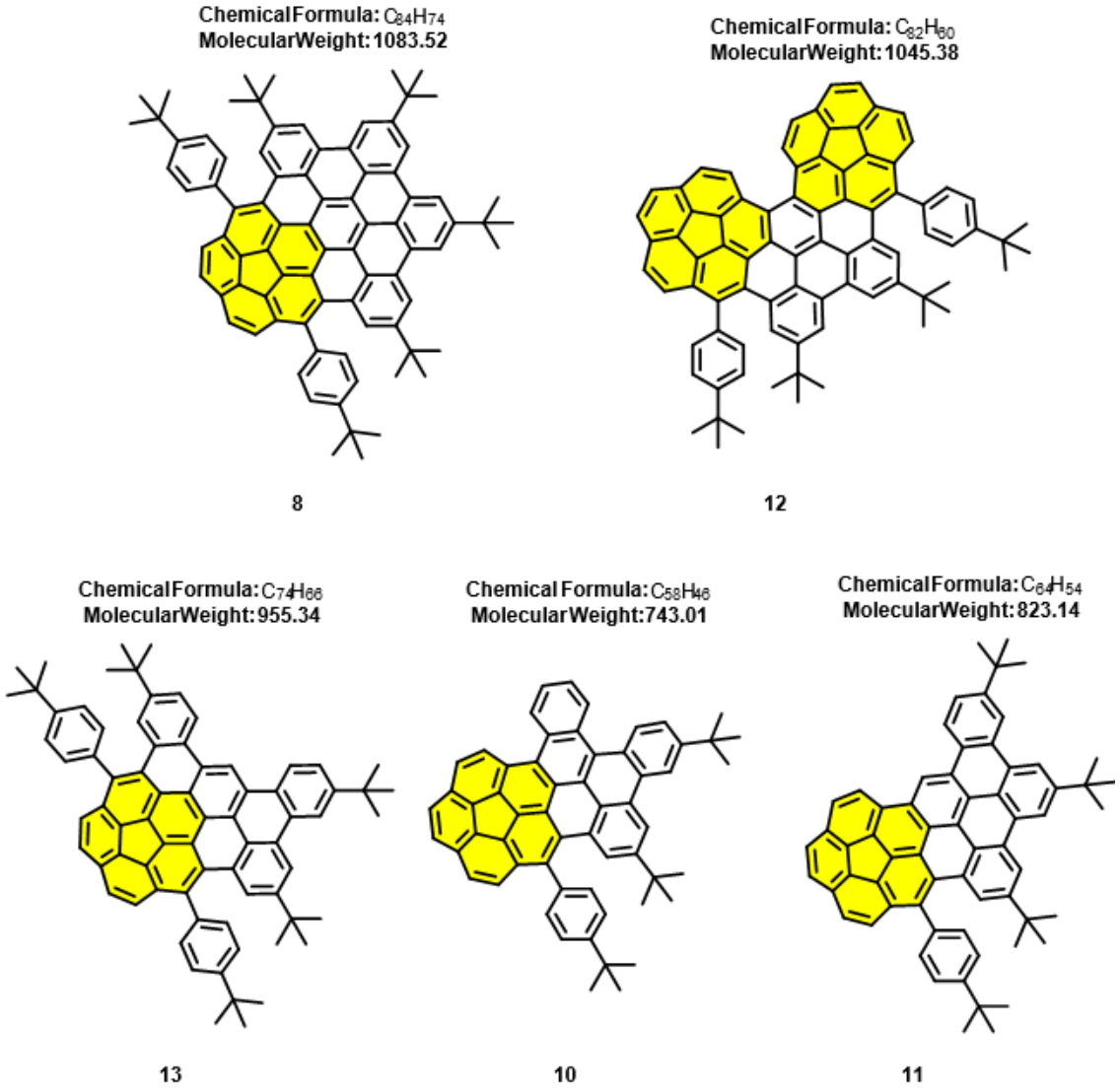

Figure 17. Structures of corannulenes with extended aromatic systems. The corannulene group is highlighted for comparison

Nevertheless, when the E^0_f-values of these corannulenes were compared to PCBM, it is apparent that the degree of electron affinity of the corannulenes (~ -2.0 V *vs.* Fc/Fc^+) are still inferior to PCBM (-0.9 V *vs.* Fc/Fc^+) by a large margin. Out of the 15 corannulenes, it can be observed from Table 1 that compounds **1** and **2** were the closest in terms of E^0_f-values to PCBM, and between the two, **2** displayed a first reduction potential at -0.84 V *vs.* Fc/Fc^+ which is even less negative than that of the state of the optimal fullerene acceptor, PCBM (**Figure 18**).

Furthermore, both compounds displayed E^0_f-values close to unity suggesting their one-electron reduced states were relatively long-lived.

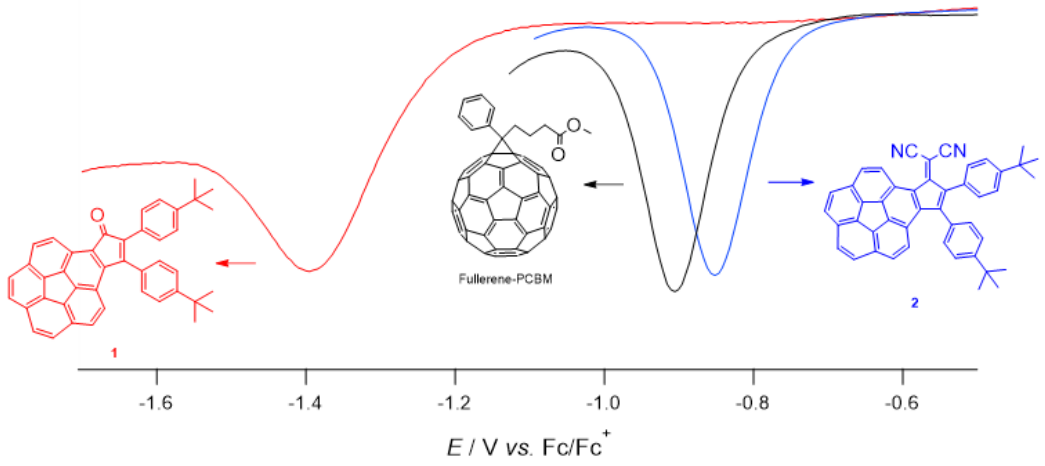

Figure 18. square-wave voltammetry comparison of the first reduction potential of PCBM and corannulenes **1** and **2**.

5.4 In situ UV-vis spectroscopy electrolysis analysis.

CV measurements in isolation only allow an estimation of lifetimes of up to a few seconds, due to the voltammetric scan rates that are used of a least 0.1 V s^{-1} and the convective-diffusive processes that occur where the solution phase molecules continually move away from the electrode surface. Therefore, controlled potential electrolysis can be used to prepare solutions of electrolysed molecules, where their lifetimes can be probed using voltammetry or spectroscopy. For compounds **1** and **2**, *in situ* electrochemical-UV-vis spectroscopy was carried out using an optically semi-transparent thin layer electrochemical (OSTLE) cell at room temperature (22 ºC ± 2ºC). As the electrolysis and UV-vis spectroscopy occur in situ, the potentials were referenced to an Ag wire reference electrode (separated by a frit from the test solution) instead of Fc/Fc^{+}. *Ex situ* CV experiments were initially conducted to determine the potential to be applied with respect to the Ag reference electrode, which was set -1.0 V vs. Ag, which was sufficiently negative to reduce the compounds by one-electron but insufficient to reach their second reduction potentials.

The UV-vis spectra obtained during the one-electron electrolysis of compounds **1** and **2** and shown in **Figure 19**. The spectra displayed several isosbestic points during electrolysis suggesting indicating one main product was being formed, that is, the radical anions.

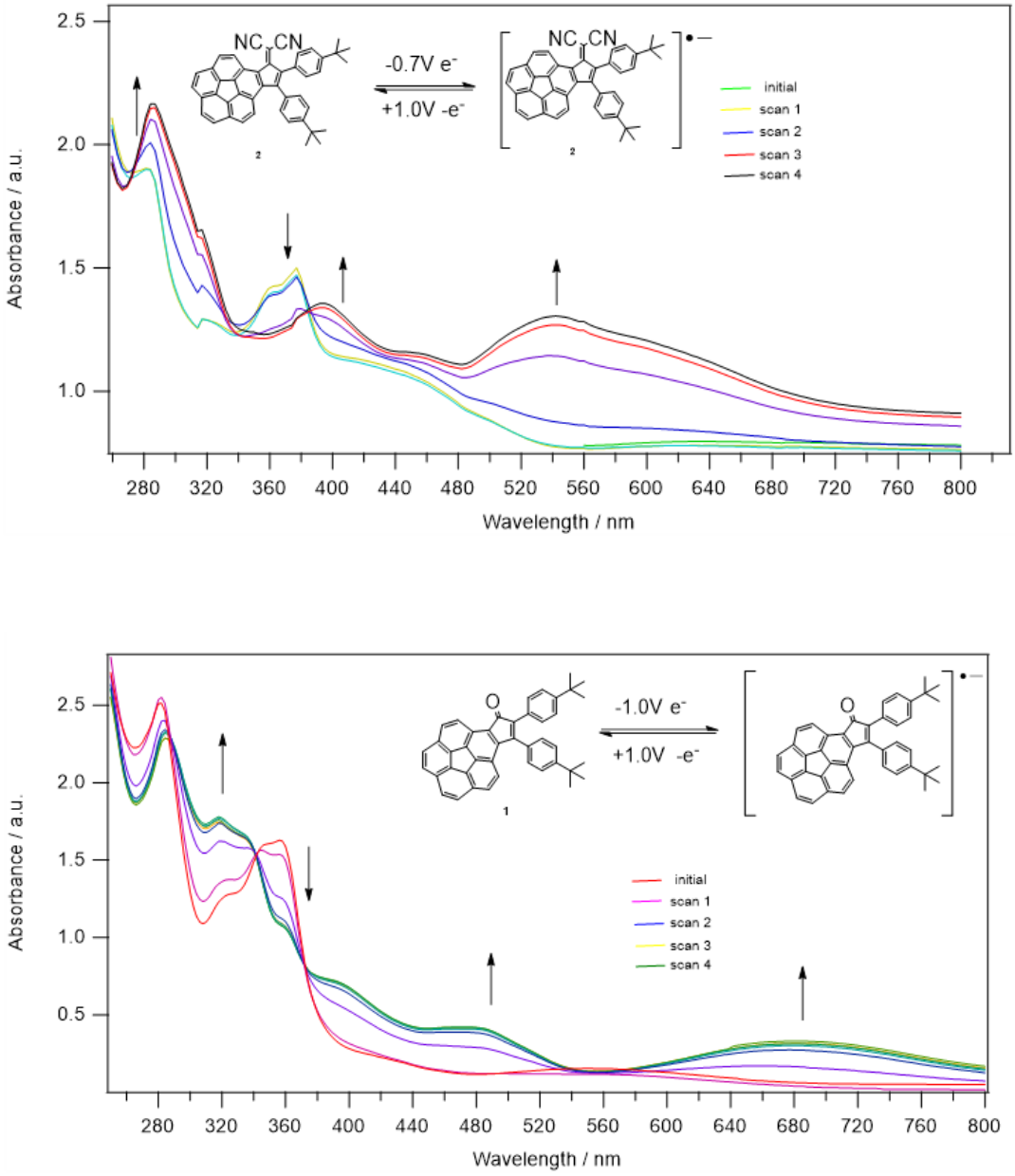

Figure 19. UV-Vis spectra obtained from the reduction of corannulene 1 and 2 at their respective first reduction potential (vs. Ag/Ag^+) and re-oxidation at +1.0V (vs. Ag/Ag^+)

For both compounds **1** and **2**, UV-vis scans were recorded until no further changes were observed in the spectra, which indicated the reduction processes were fully completed. Both compounds displayed a large increase in absorbance from 480 nm to 720 nm range while converting into their radical anion forms, suggesting additional lower energy transitions for the

radical anions. This is likely due to the unpaired electron existing in a higher energy HOMO (compared to the diamagnetic starting material), thus the transition to the first electronic excited state requiring less energy than the starting material.

Both radical anion species of compounds **1** and **2** were able to be re-oxidized back to the starting material by applying a potential of 0 V *vs.* Ag wire after first reducing them. This indicates that radical anions of **1** and **2** were stable enough to not decompose or react in the solution state over a period of several hours, thus giving them promising prospects in applications as stable electron acceptors.

In situ electrochemical-UV-vis experiments were also performed on compounds **1** and **2** by applying a potential sufficiently negative to cause the transfer of a second electron. Compound **1** showed limited stability during the second reduction process and was unable to be re-oxidized back into the starting material. On the other hand, compound **2** was found to be able to undergo a second one-electron reduction to generate a dianion which was stable long-lived enough to be able to be re-oxidized back into the starting material **2**, which was proven by the regeneration of the UV-vis spectrum of **2** upon applying a positive potential (**Figure 20** and **21**).

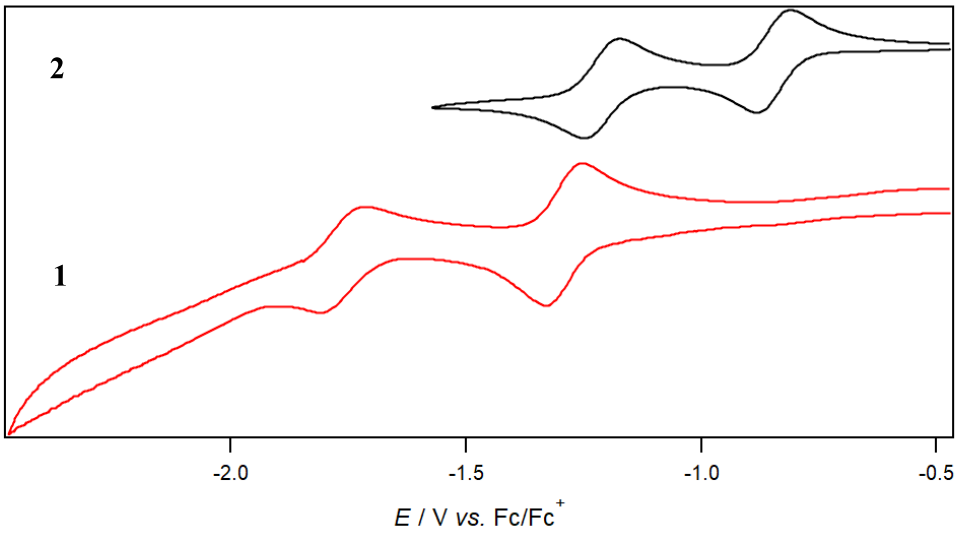

Figure 20. Illustration of corannulene **1** and **2**'s ability to undergo a second reversible reduction peak

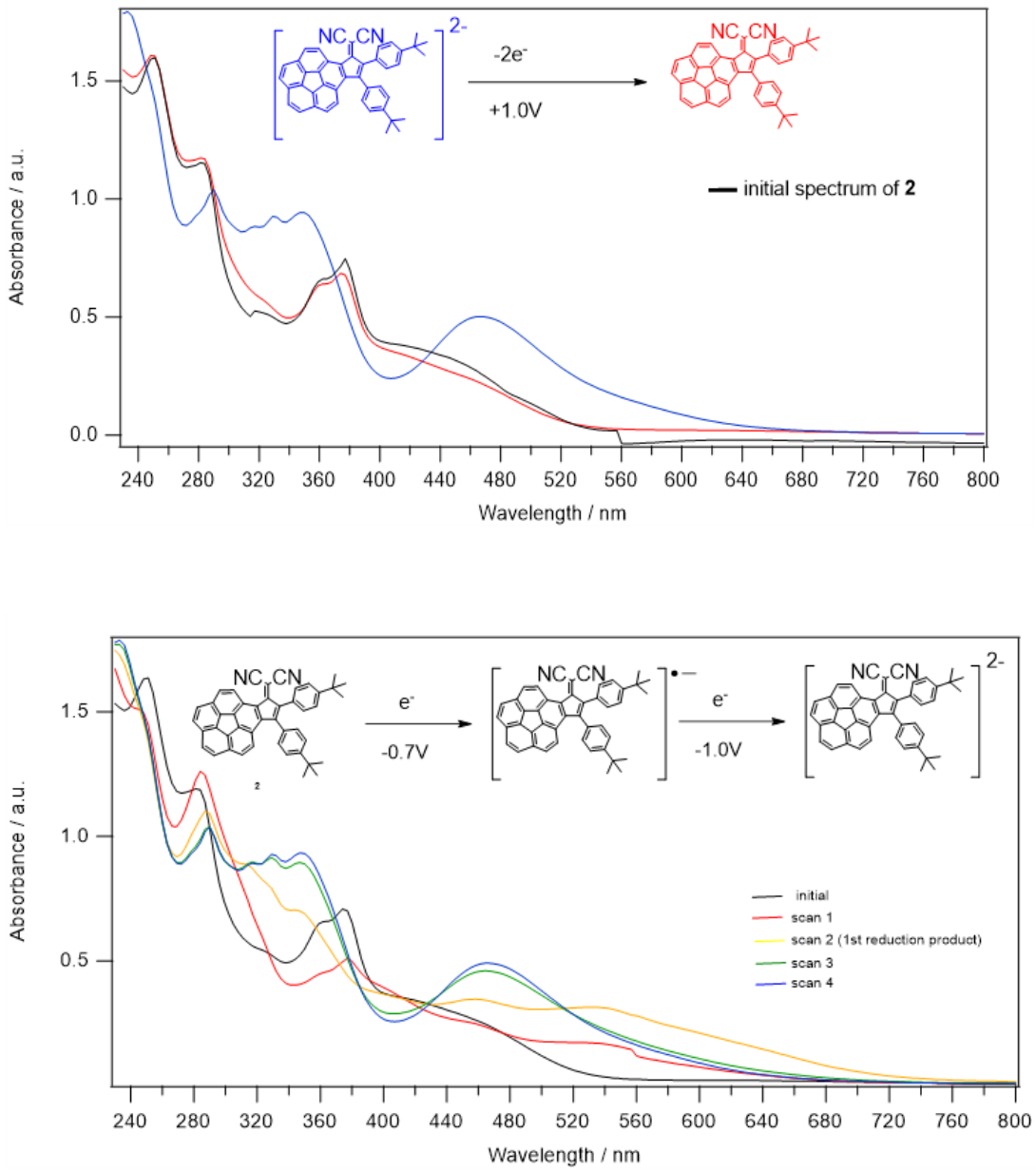

Figure 21. UV-Vis spectra obtained from the reduction of corannulene **2** at its second reduction potential -1.0V(vs. Ag/Ag^{+}) and re-oxidation at +1.0V (vs. Ag/Ag^{+})

5.5 Confirmation of radical species using EPR spectroscopy

Ex situ EPR spectroscopy was conducted on solutions of compounds **1** and **2** that were exhaustively electrolysed by one-electron under argon and then transferred into an EPR flat cell. In both cases the electrolysed solutions produced intense single line EPR spectra (**Figure 22** and **23**), with *g*-values close to 2.00 characteristic of organic radicals with signals close to the free electron value. The lack of hyperfine structure is a common feature in radicals of corannulene-based compounds, while the EPR spectra do confirm the paramagnetic nature of the one-electron reduced species.

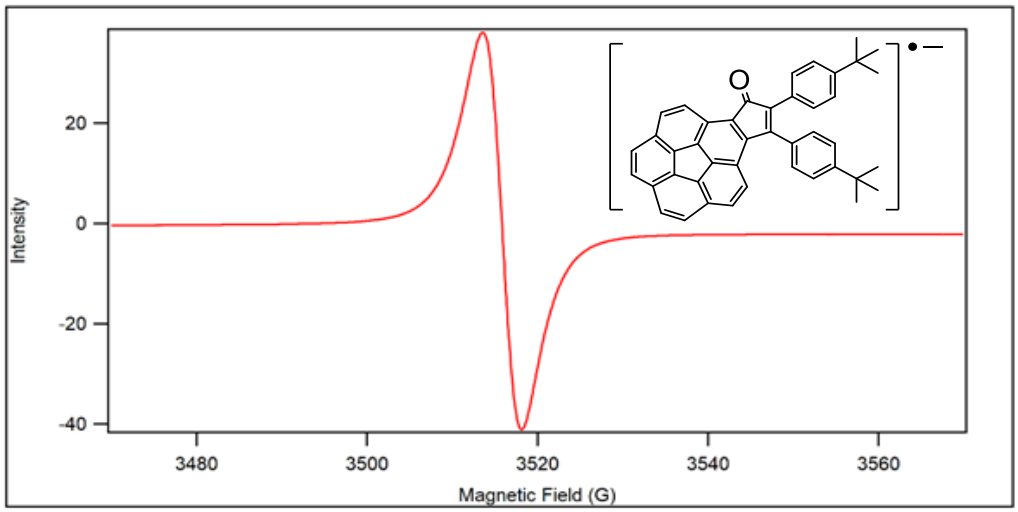

Figure 22. EPR spectrum of corannulene **1** after electrolysis has taken place at its corresponding first reduction potential.

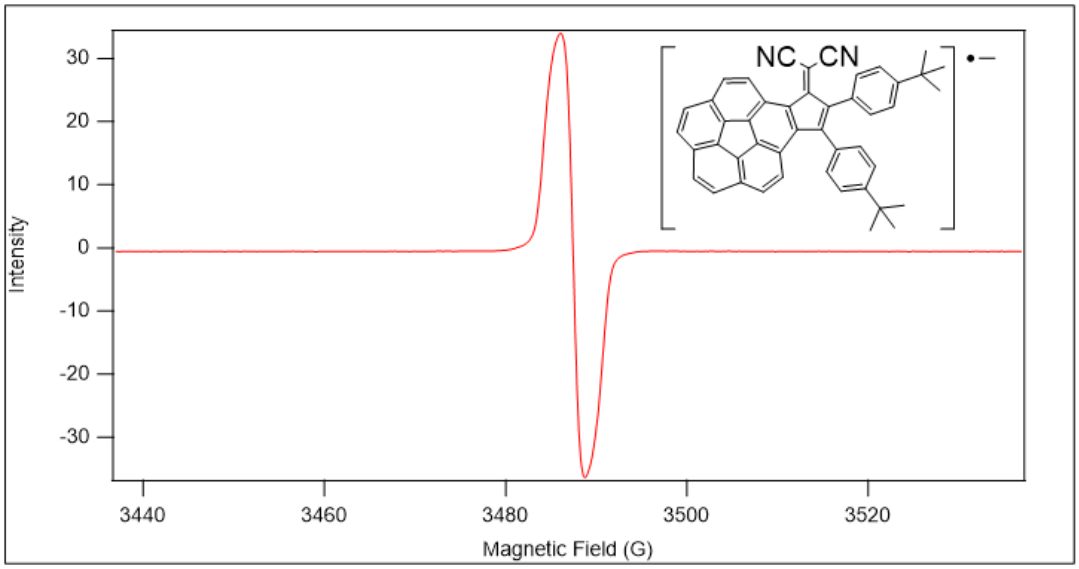

Figure 23. EPR spectrum of corannulene **2** after electrolysis has taken place at its corresponding first reduction potential.

5.6 Summary

This chapter reports the electrochemical characterization of several novel corannulene derivatives. Among these, compound **2** exhibits particularly promising properties for application as an electron acceptor. Comprehensive characterization, including electrochemical analysis and in situ UV vis spectroscopic methods paired with electrolysis, validates that compound **2** possesses both high electron affinity, approaching or exceeding that of the benchmark fullerene derivative PCBM, and exceptional electrochemical stability. This represents the first documented instance of a corannulene derivative based on the best of our knowledge achieving electron affinity within this regime.

The combined attributes of high electron affinity and robust radical anion stability position compound **2** as a highly promising candidate for organic photovoltaics (OPVs). Corannulene derivatives offer significant potential advantages over traditional fullerenes like PCBM, notably in terms of enhanced synthetic tunability, allowing for deliberate structural modification to optimize properties such as absorption, energy levels, and solid-state packing – and potentially improved synthetic accessibility and scalability.

5.7 References

1. G, Shao.;. Work function and electron affinity of semiconductors: Doping effect and complication due to fermi level pinning. *Energy. Environ. Mater.* **2021** *4*(3), 273-276.

2.J. C. Rienstra-Kiracofe,; G. S. Tschumper,; H. F. Schaefer,; S. Nandi,; G. B. Ellison. Atomic and molecular electron affinities: photoelectron experiments and theoretical computations. *Chem.Rev.* **2002** *102*(1), 231-282.

Chapter 6. Conclusions and Recommendations

6.1 General conclusions

6.2 Challenges and recommendations for future research

6.1. General conclusions

This thesis investigates the current amplification of BPA through the modification of electrode surfaces, as well as the electrochemical characterization based on the electron affinity behavior of multiple corannulene-based derivatives.

Firstly, pronounced oxidative peak current amplification (i_p^{ox} > 1000 μA) observed for bisphenol A (BPA) detection using a glassy carbon electrode (GCE) modified with a nanocomposite of carboxyl-functionalized multi-walled carbon nanotubes (fMWCNTs-COOH), magnetite nanoparticles (Fe_3O_4), and polyvinylpyrrolidone (PVP) surfactant is investigated. This significant amplification is primarily hypothesized to result from a pseudo-electrochemical-catalytic cycle, where the Fe_3O_4 nanoparticles continuously recycle BPA by reducing its oxidized intermediates (1+/2+ species) back to BPA during cyclic voltammetry at the cost of losing trace iron particles through Fe^{2+}. The PVP surfactant plays a critical multifaceted role of significantly reduces agglomeration and holding the composite materials in place, leading to enhanced porosity, uniform electrode coverage, and increased electroactive surface area. Furthermore, PVP promotes favourable ion-dipole interactions between the electronegative oxygen atoms in its structure and the cationic oxidized BPA species, bringing the analyte closer to the catalytic Fe_3O_4 interface. The homogeneous distribution of Fe_3O_4 catalytic sites and pervasive mobile electron pathways within the composite, confirmed by EDX mapping, ensure efficient electron transfer via the conductive fMWCNTs-COOH network surfaces. Therefore, the fMWCNTs-COOH/Fe_3O_4/PVP nanocomposite could potentially function as a highly effective sensing platform for BPA detection.

Also, using multiple electrochemical techniques such as cyclic voltammetry, square-wave voltammetry, and in-situ UV-vis electrolysis, several new corannulene compounds were examined and with compound **2** characterized to possess both high electron affinity and

electrochemical stability, which is comparable, or even better than that of the most widely used fullerene-based compound, PCBM. This is the first time a corannulene is reported to exhibit electron affinity in this regime and shows promising applications in the field of organic photovoltaics with the advantage in terms of tunability and productivity. However, applications of electron acceptors are often in conjunction with complex systems and many other variables such as donor compatibility and chemical erosion have to be considered, which can only be confirmed through direct practical tests.

6.2 Further recommendations for future research

Starting with BPA current amplification, Future research should focus on achieving lower and more reproducible limits of detection (LOD) through optimized electrode modification protocols to enable trace-level environmental BPA monitoring. There are also many challenges when trying to link to real-world application, including developing robust antifouling strategies to mitigate matrix interference from complex samples like biological fluids or soil leachates. Also, comprehensive studies on long-term stability under repeated use and scalable nanomaterial production for cost-effectiveness are essential to advance this technology toward practical implementation.

Another major challenge and limitation faced by electrochemical portable devices is electrode fouling. Signal decay can be observed when interferences such as proteins, polysaccharides, and lipids adsorb onto the electrode surface, when performing analysis on biological samples such as food/body fuids/water, which often are concerns of BPA leaching. These interferents could form insulating layers which drastically reduces electron transfer kinetics between BPA and the electrode. Common interferences include albumin, ascorbic acid, and other phenols, which can be found commonly in water/food samples.

In order to tackle this problem, we could aim to introduce a selective layer that blocks large interferents (like proteins) while allowing small target molecules (like BPA) to pass through, at the surface of electrode. This could be potentially achieved by implementing hydrogels like PEG as the alternative to PVP surfactant where a hydrated, bio-inert layer that is extremely resistant to protein adsorption can be formed. However, the electroconductivity of such hydrogel has to be further optimized, perhaps by introducing zwitter-ionic groups such as poly(sulfobetaine methacrylate) - pSBMA

For the corannulene project, the promising intrinsic properties of compound **2** possessing high electron affinity and robust radical anion stability, position it as a compelling candidate for organic photovoltaics (OPVs), potentially rivalling or surpassing benchmark acceptors like PCBM. However, translating these molecular attributes into viable device performance necessitates confronting significant application testing challenges. The foremost challenge lies in the complex, system-dependent nature of functional OPV devices. Successful integration requires rigorous experimental validation far beyond fundamental electrochemical characterization. For example in the area of establishing compatible donor-acceptor pairings, where energy level alignment must facilitate efficient charge transfer. Predicting these interactions remains difficult, demanding empirical screening with diverse polymeric donors. Which should be a primary focus in expanding on this project into its application potentials

Despite these testing complexities, the inherent chemical tunability of the corannulene scaffold offers a strategic pathway forward. Future efforts can leverage this adaptability to systematically design derivatives targeting enhanced compatibility, stability, and processability.

Supporting Information

Contents

Page S15 ***Figure S10.*** (*a-e*) TEM images of f-MWCNTs/FeNPs/PVP. (*f*) Size distribution histogram from TEMs. Sample size collected: 90. Mean size: 91.1 nm. SD: 29.2 nm. Min.: 52.0 nm. Max.: 157.3 nm.

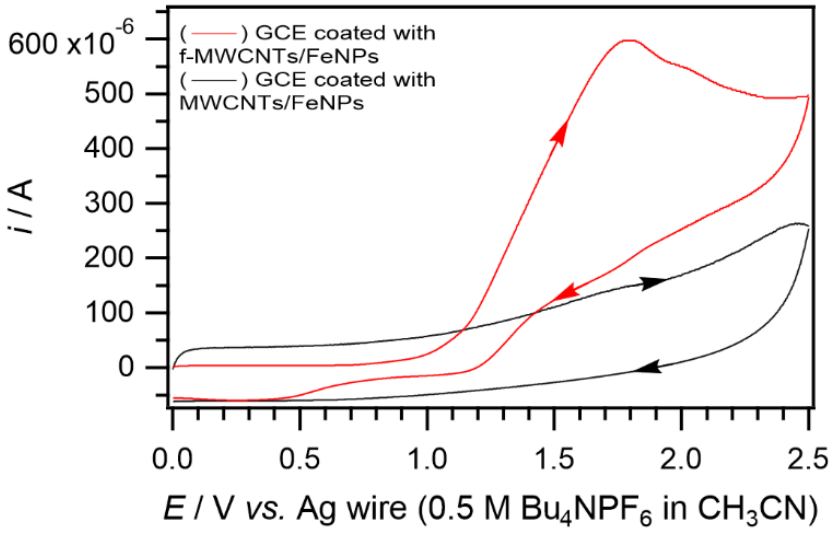

Figure S1. Cyclic voltammograms of 1 mM BPA in CH_3CN containing 0.5 M *n*-Bu_4NPF_6 at a scan rate of 0.1 V s^{-1} at a 3 mm diameter GC electrode coated with -COOH functionalized multiwalled carbon nanotubes (f-MWCNTs) combined with FeNPs, and non-functionalized multiwalled carbon nanotubes (MWCNTs) combined with FeNPs, at 22 ± 2ºC.

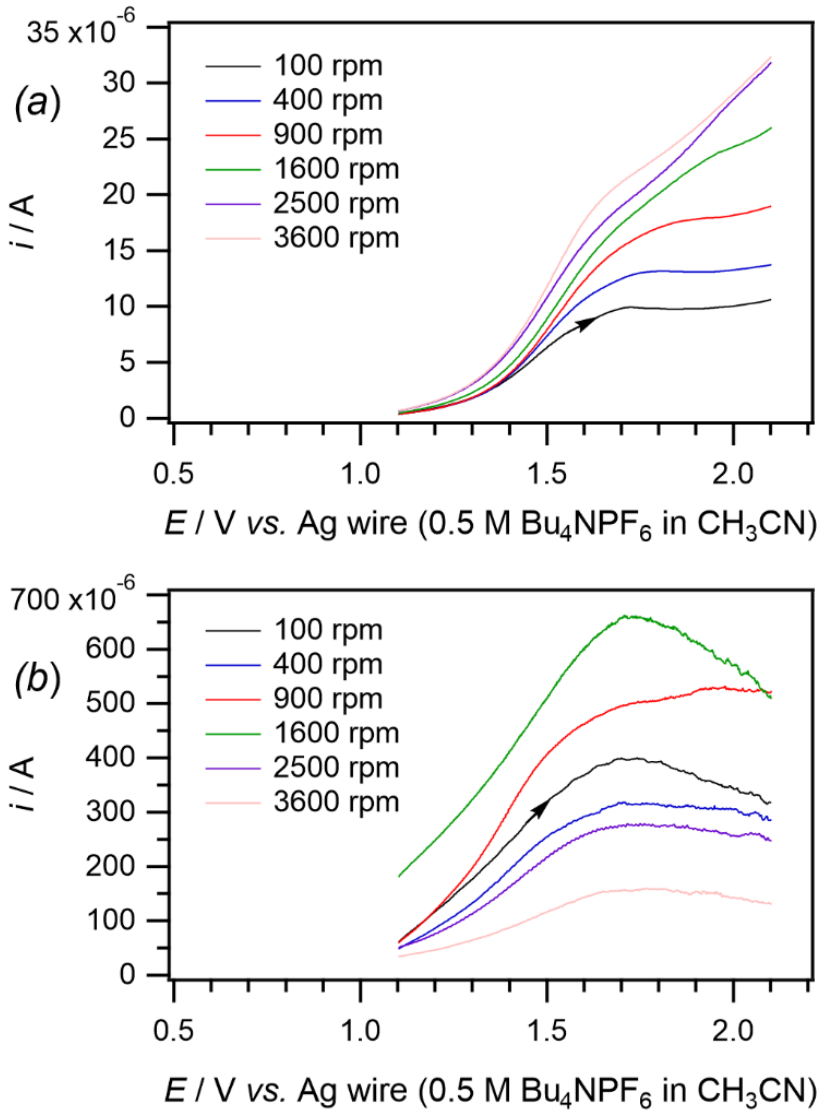

Figure S2. Linear sweep rotating disk electrode experiments performed on a 3 mm diameter electrode at a scan rate of 50 mV s^{-1} in CH_3CN containing 1 mM BPA and 0.5 M *n*-Bu_4NPF_6 at 22 ± 2ºC. (*a*) GC electrode (*b*) GC electrode coated with f-MWCNTs/FeNPs/PVP composite.

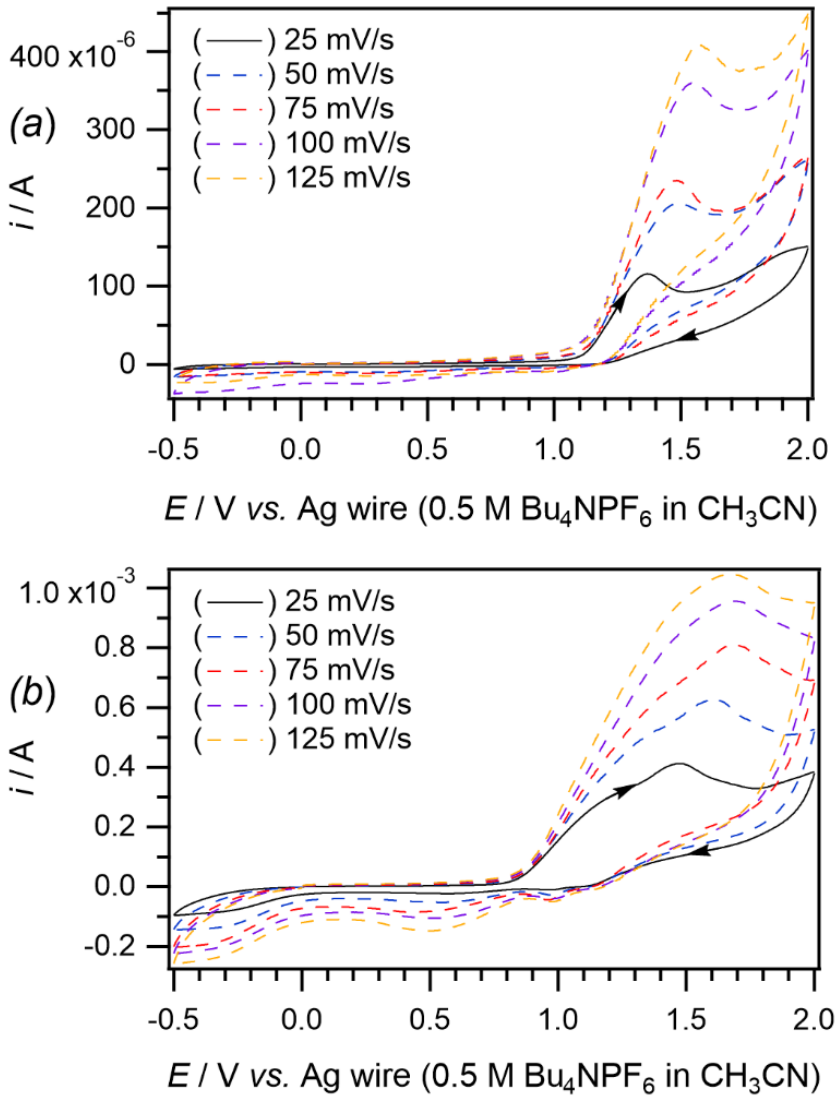

Figure S3. Cyclic voltammograms of 1 mM BPA in CH_3CN containing 0.5 M *n*-Bu_4NPF_6 at a 3 mm diameter electrode at 22 ± 2°C at variable scan rates. (*a*) GC electrode (*b*) GC electrode coated with f-MWCNTs/FeNPs/PVP composite.

(*a*)

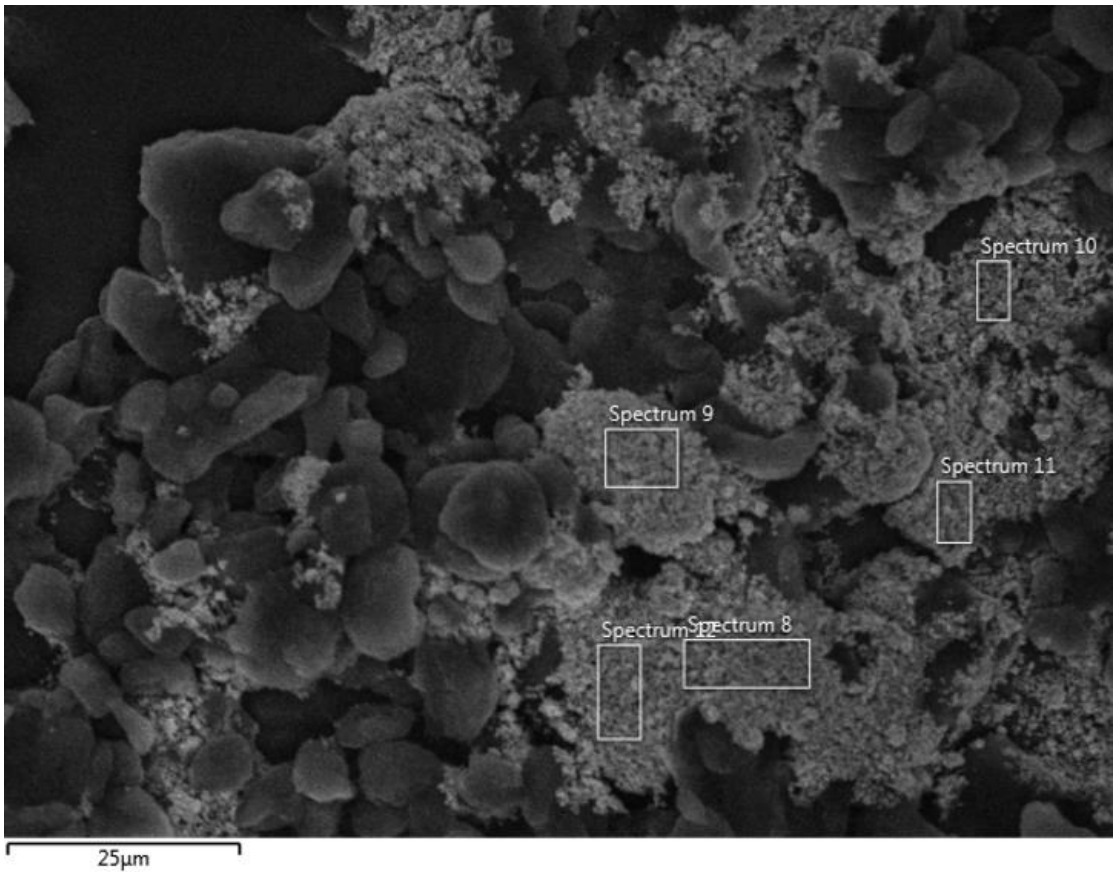
Spectrum 10
Spectrum 9
Spectrum 11
Spectrum 8
25µm

(*b*)

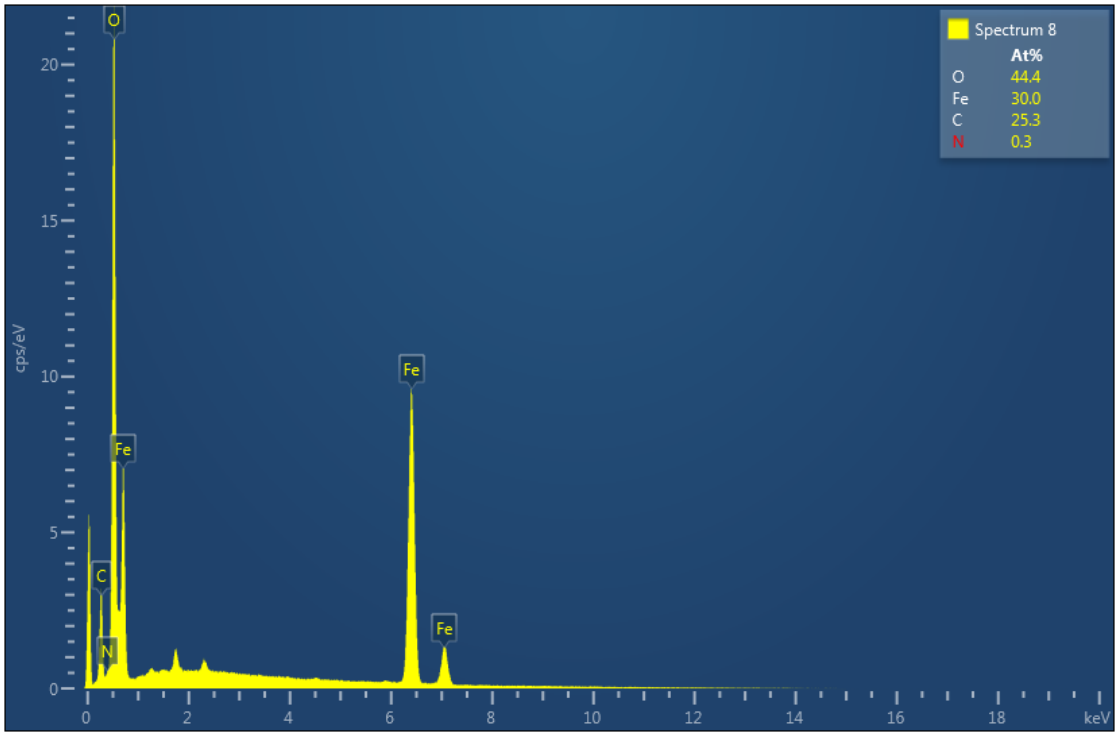
Spectrum 8
At%
O 44.4
Fe 30.0
C 25.3
N 0.3
O
Fe
C
N
Fe
Fe
cps/eV
keV

(*c*)

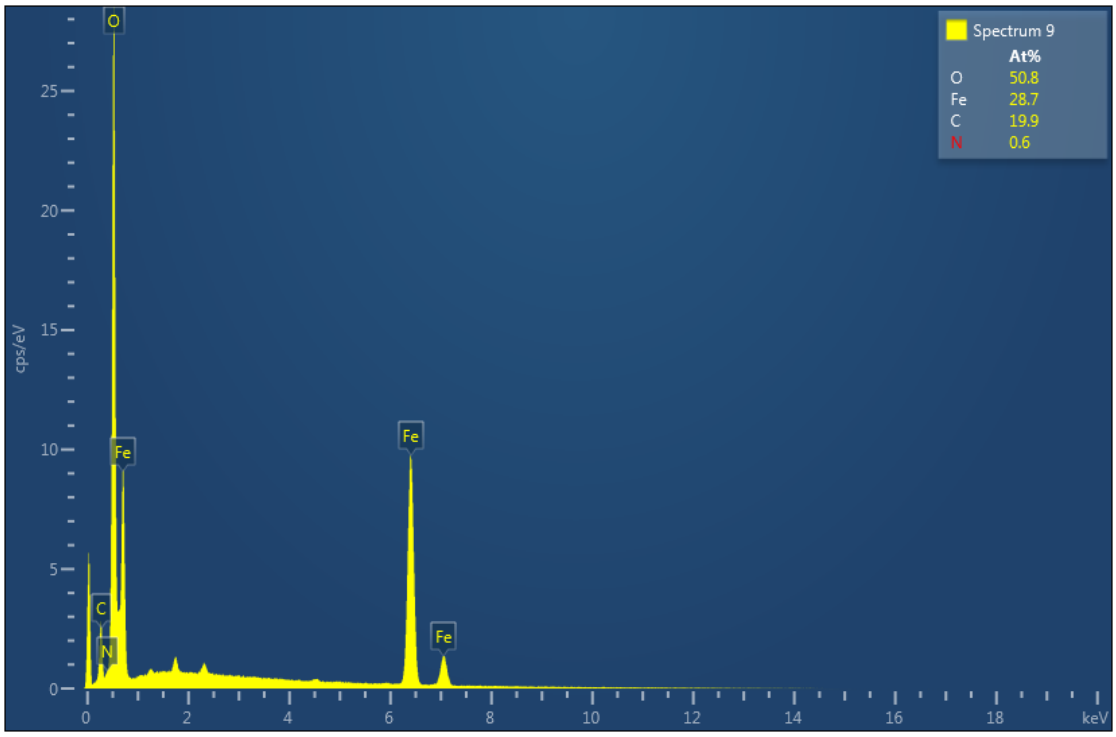
Spectrum 9
At%
O 50.8
Fe 28.7
C 19.9
N 0.6
cps/eV
keV
O
Fe
Fe
C
N
Fe

(*d*)

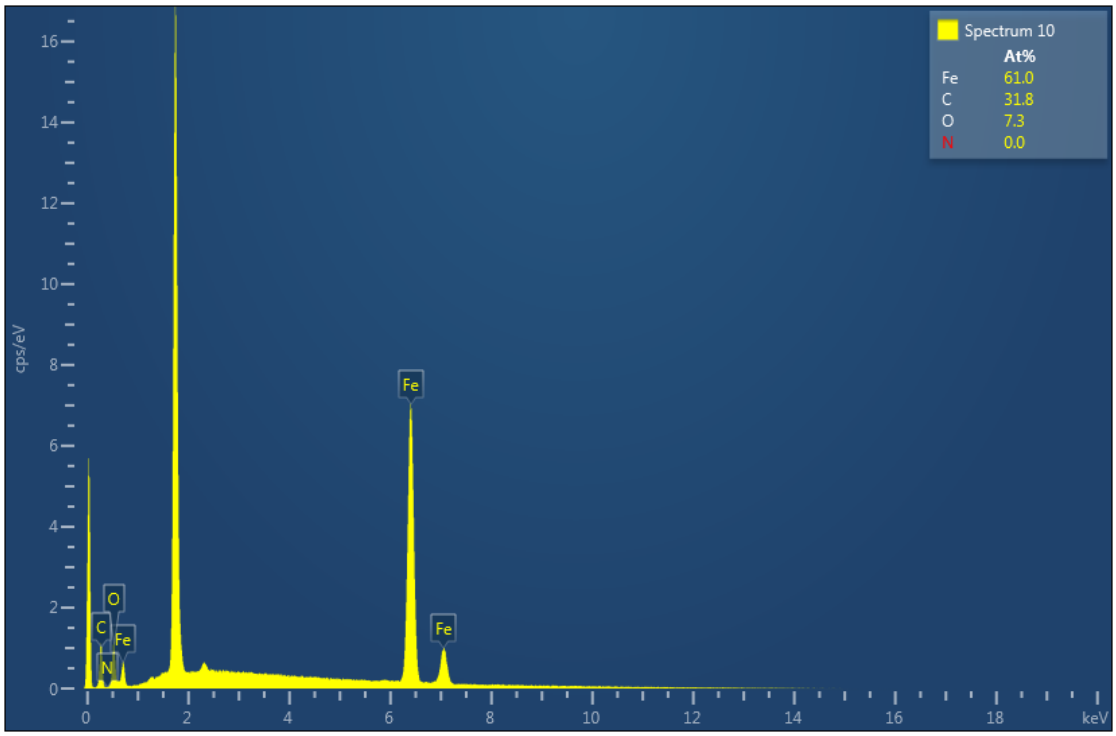
Spectrum 10
At%
Fe 61.0
C 31.8
O 7.3
N 0.0
cps/eV
keV
Fe
O
C
Fe
N
Fe

(*e*)

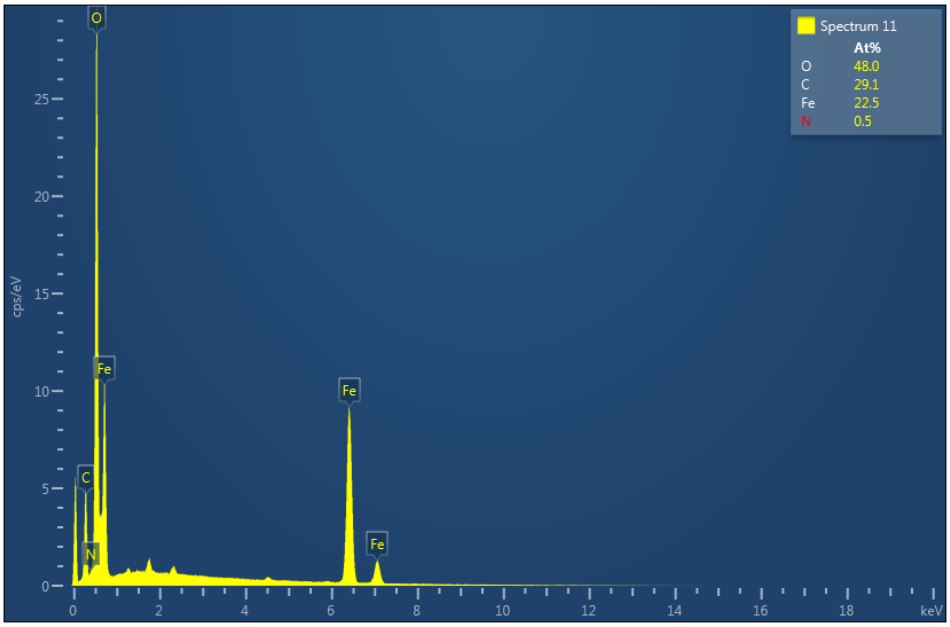

(*f*)

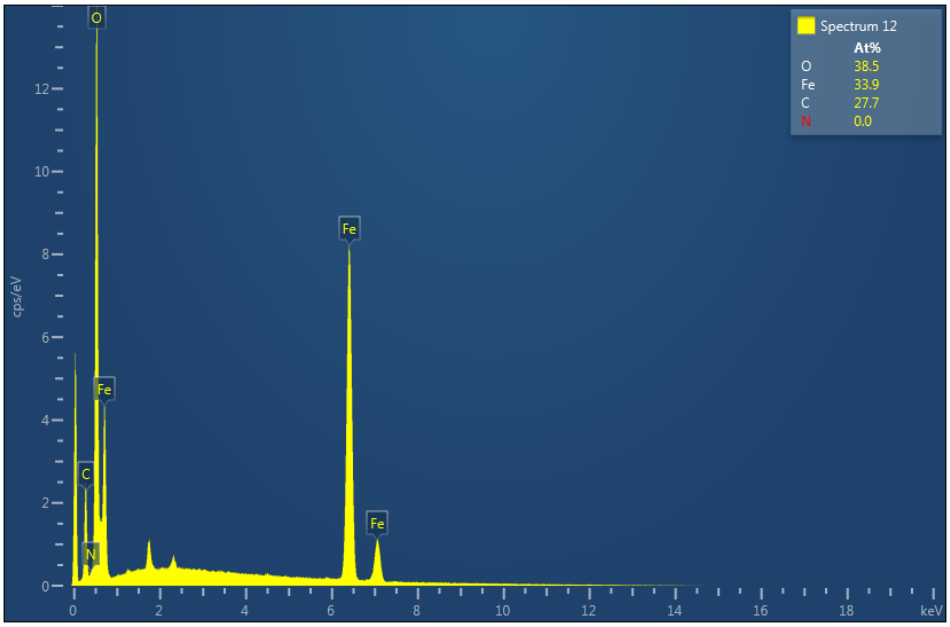

Figure S4. Images, composition and atomic distribution of f-MWCNTs/FeNPs without PVP surfactant. (*a*) SEM images. (*b-f*) EDX spectra from different portions of SEM image. *Description:* The EDX spectra quantitatively reveal the elemental composition and distribution across the f-MWCNTs/FeNPs composite structure. Oxygen (O) dominates the atomic percentage, due to the stoichiometric abundance from Fe_3O_4, as well as the functionalization of the f-MWCNTs. Iron (Fe) appears as the only metallic component, corresponding to the nanoparticles. The atomic composition for carbon (C) is similar to that of Fe probably due to

the 1:1 Fe:C ratio during sample preparation. Crucially, the absence of PVP surfactant is represented by trace detectable nitrogen (<0.5%), likely to be from residual DMF solvent. No other trace elements were present indicating a pure composite later comprising only FeNPs and f-MWCNTs.

(*a*)

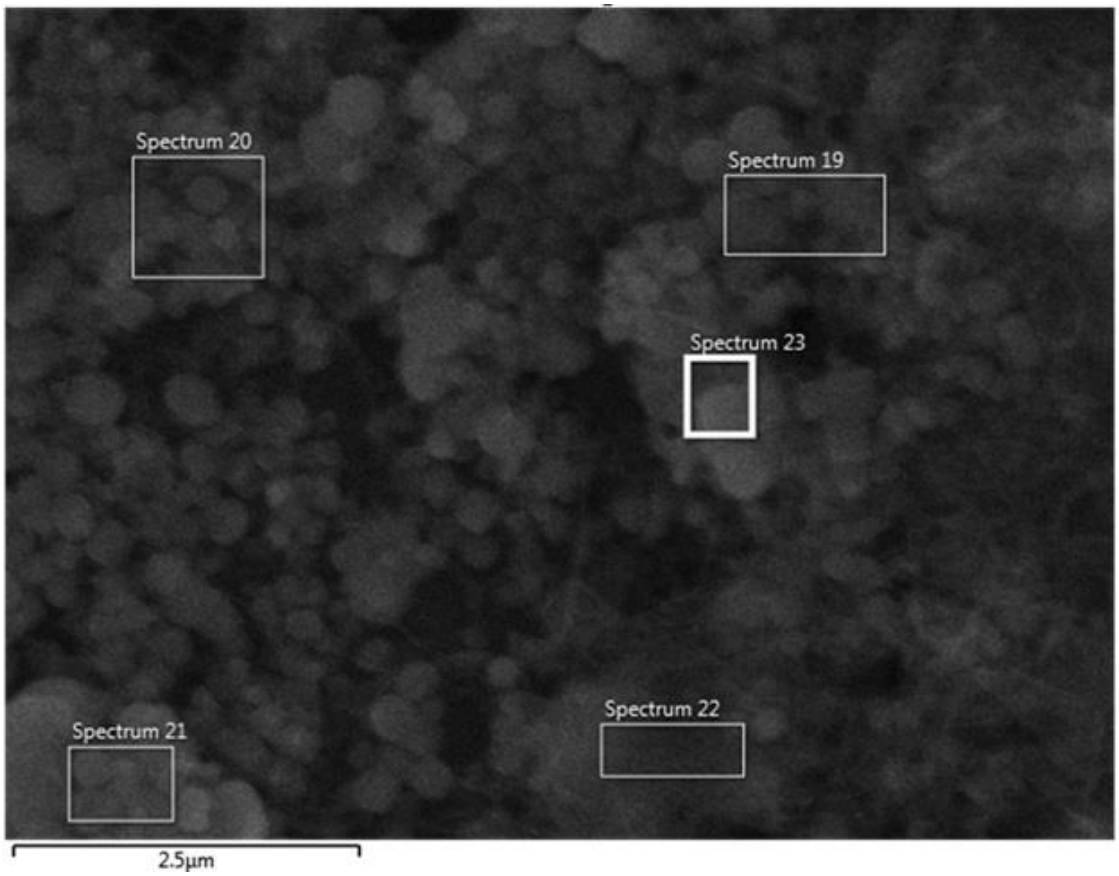

(*b*)

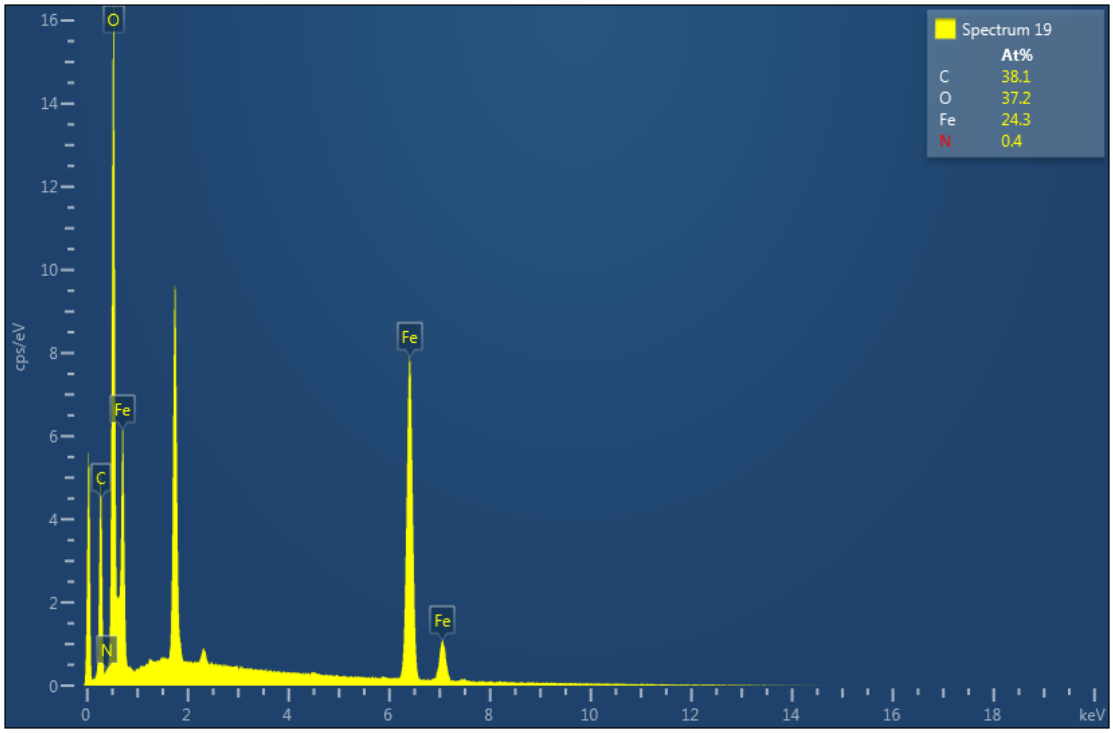
Spectrum 19
At%
C 38.1
O 37.2
Fe 24.3
N 0.4
O
Fe
C
N
Fe
Fe
cps/eV
keV

(*c*)

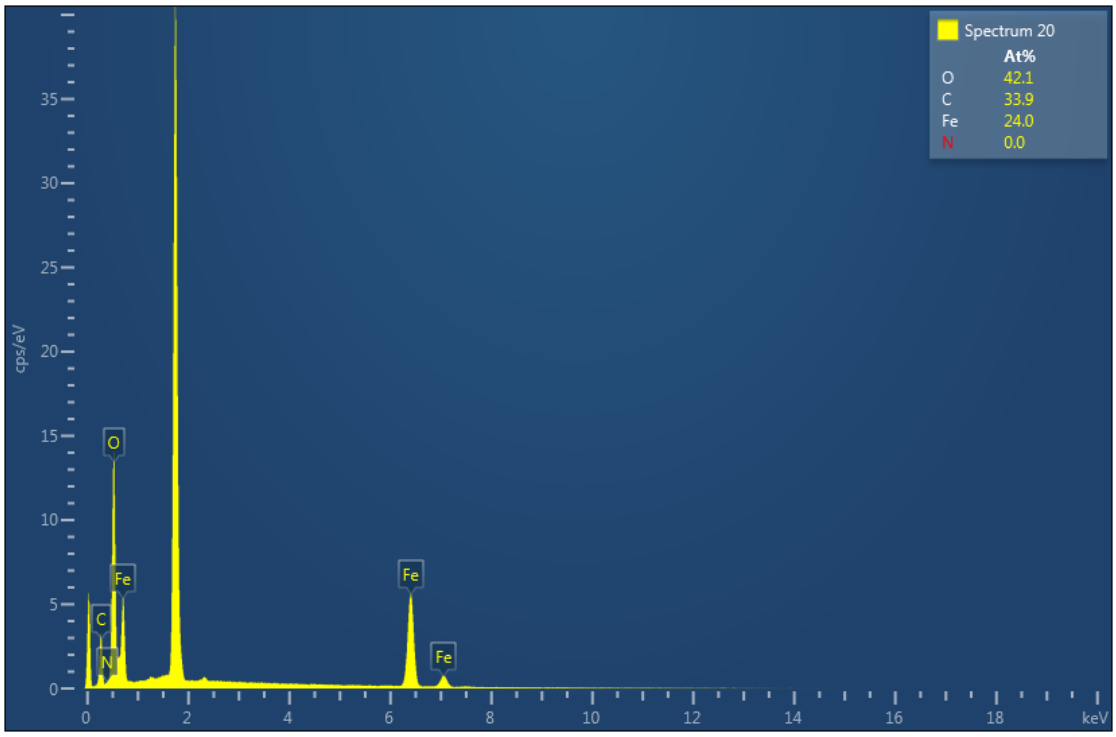
Spectrum 20
At%
O 42.1
C 33.9
Fe 24.0
N 0.0
cps/eV
O
Fe
C
N
Fe
Fe
keV

(*d*)

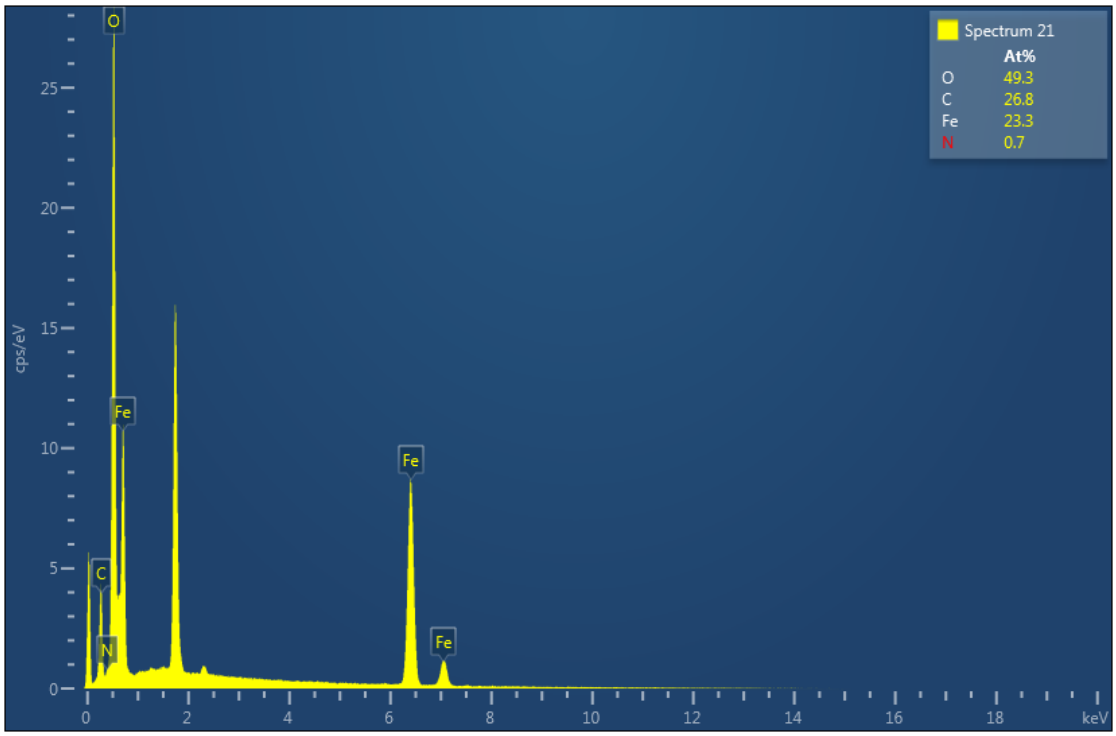
Spectrum 21
At%
O 49.3
C 26.8
Fe 23.3
N 0.7
cps/eV
O
Fe
C
N
Fe
Fe
keV

(*e*)

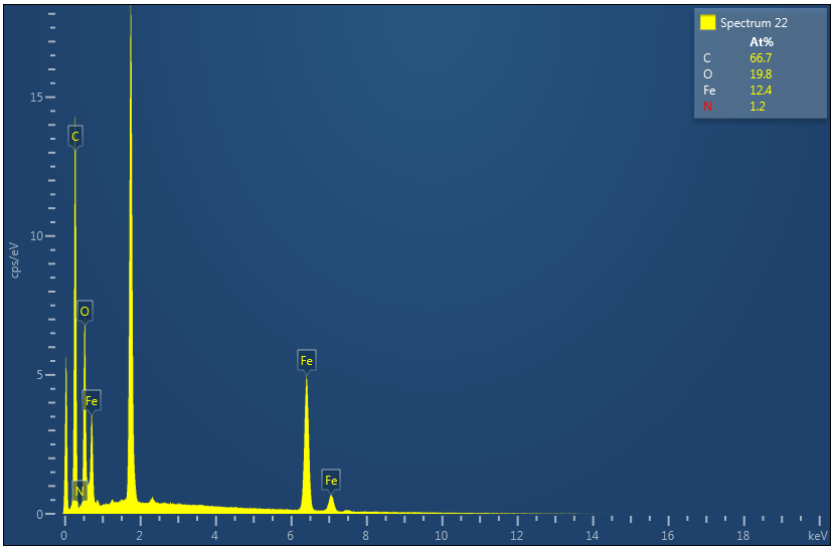

(*f*)

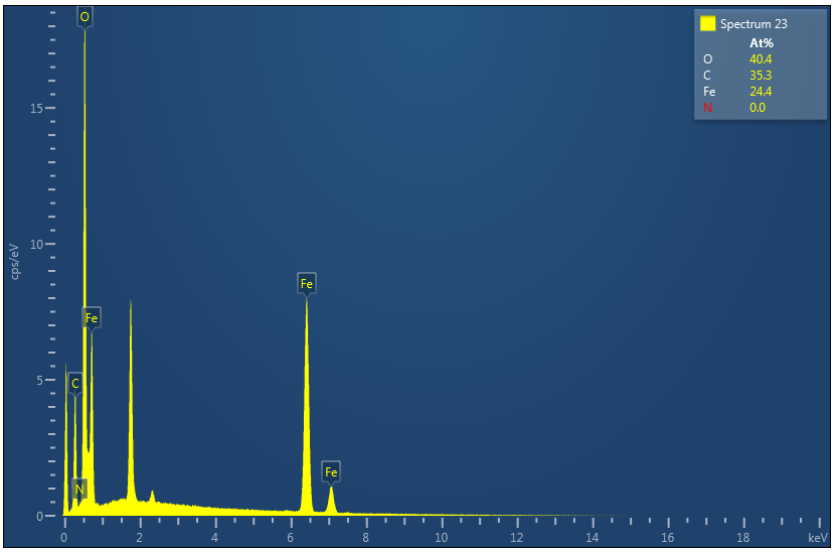

Figure S5. Images, composition and atomic distribution of f-MWCNTs/FeNPs with PVP surfactant. (*a*) SEM images. (*b-f*) EDX spectra from different portions of SEM image. *Description:* The EDX spectra quantitatively reveal the elemental composition and distribution across the f-MWCNTs/FeNPs/PVP composite. An increase in C composition is observed generally in all the spectrums, as compared to EDS analysis of the composite without PVP (from < 30% abundance to > 30% abundance). This elevation is due to the introduction of more C atoms from PVP. C and O are the two dominant elements present, due to the stoichiometric abundance from Fe_3O_4, as well as the C from PVP. Fe appears as the only metallic component, corresponding to the iron nanoparticles. The atomic composition for C is more than 1:1 the ratio of Fe as compared to EDS spectra without the addition of PVP. From the different

spectrums, particularly spectrum 22, the presence of N at 1.2% is detected from PVP, which is much higher than the trace amount detected in spectrums 8-12 in Figure S4 (without PVP) due to residual DMF solvent. It is also evident that PVP may not be evenly distributed on different parts of the electrode surface, as N appears absent in spectrums 20 and 23.

(*a*)

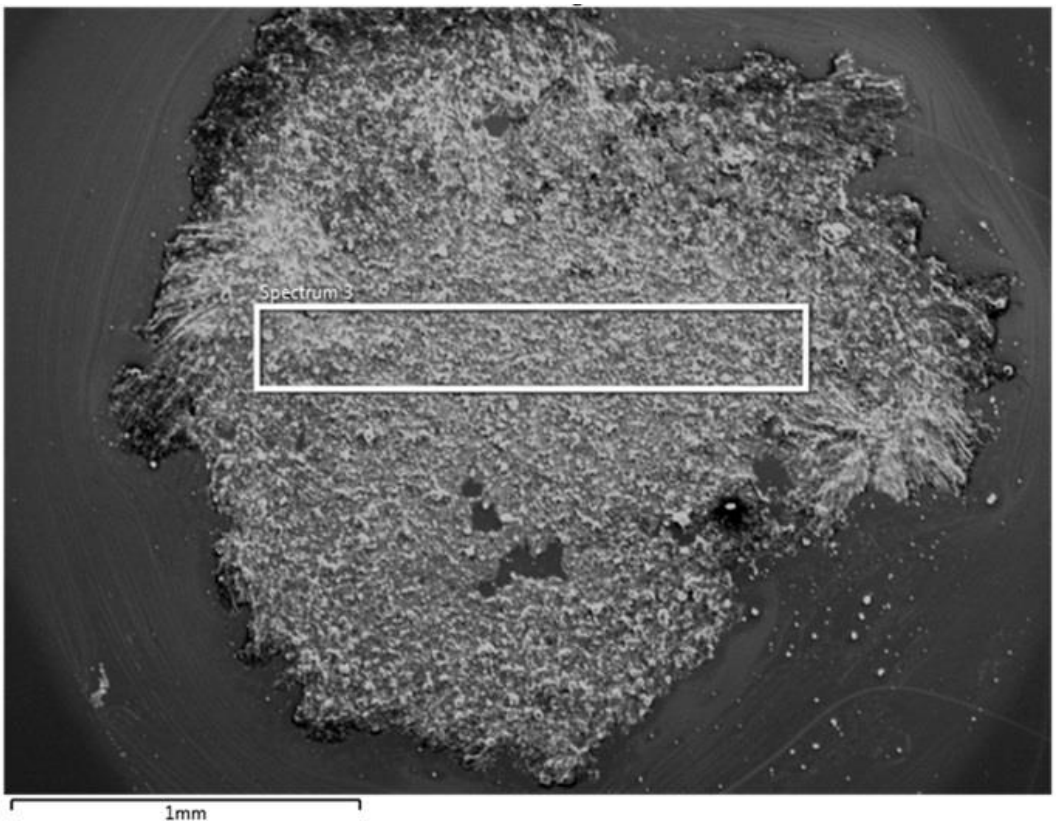

(*b*)

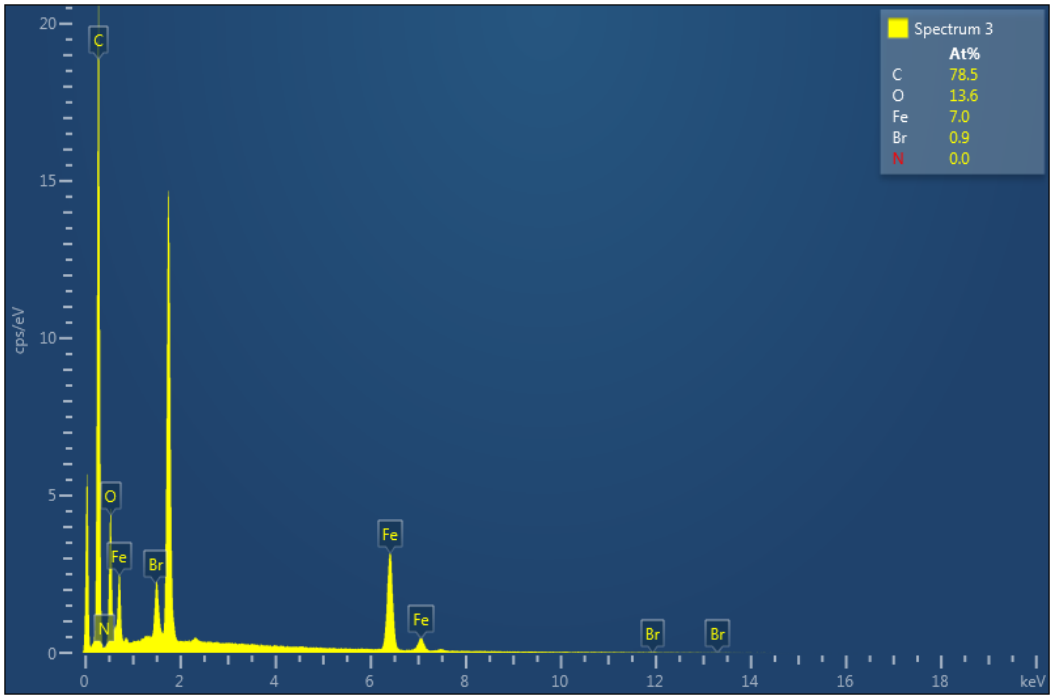

Figure S6. Images, composition and atomic distribution of f-MWCNTs/FeNPs with PVP surfactant. (*a*) SEM images. (*b*) EDX spectra from extended portion of SEM image.

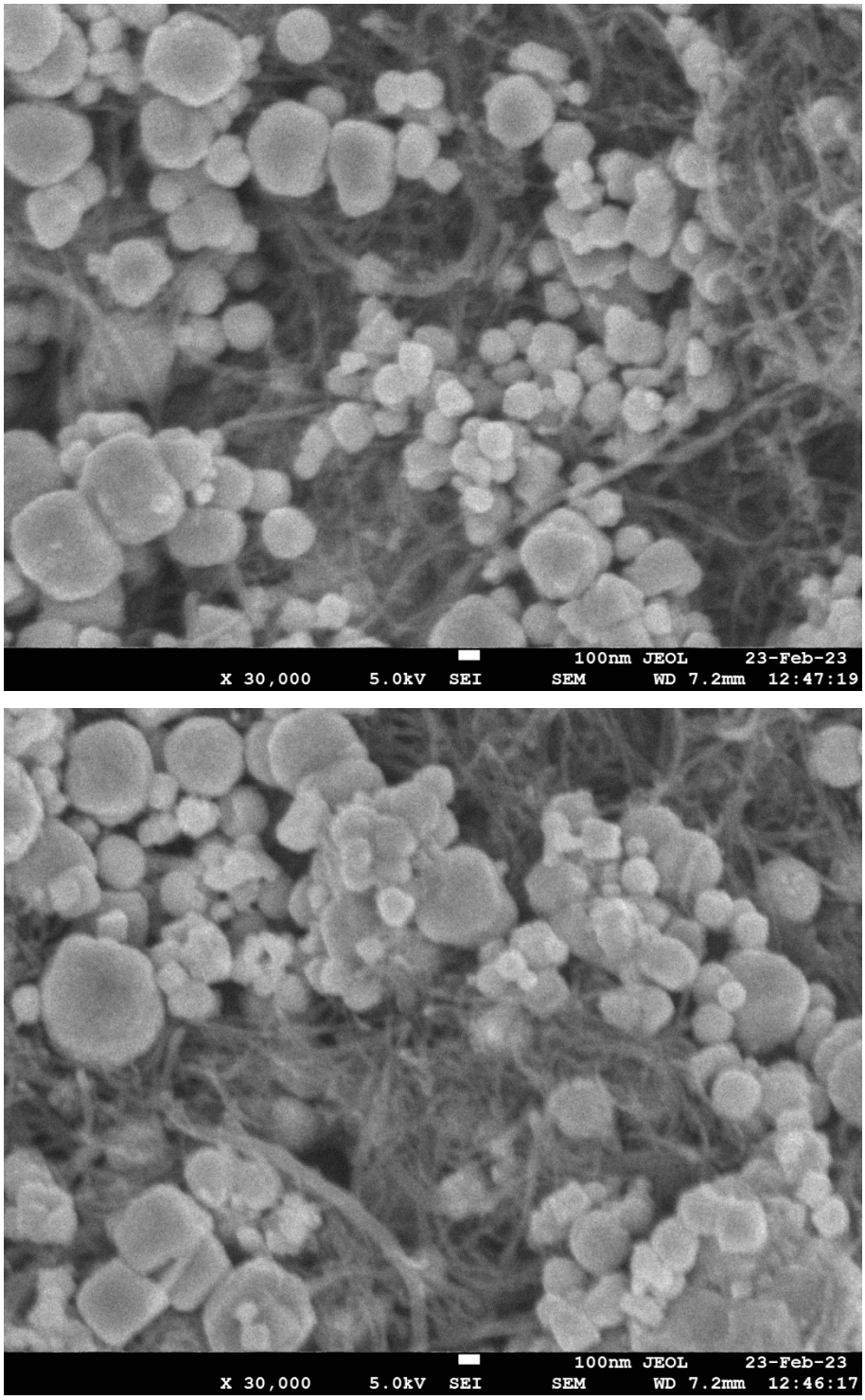

Figure S7. SEM images of f-MWCNTs/FeNPs/PVP composite.

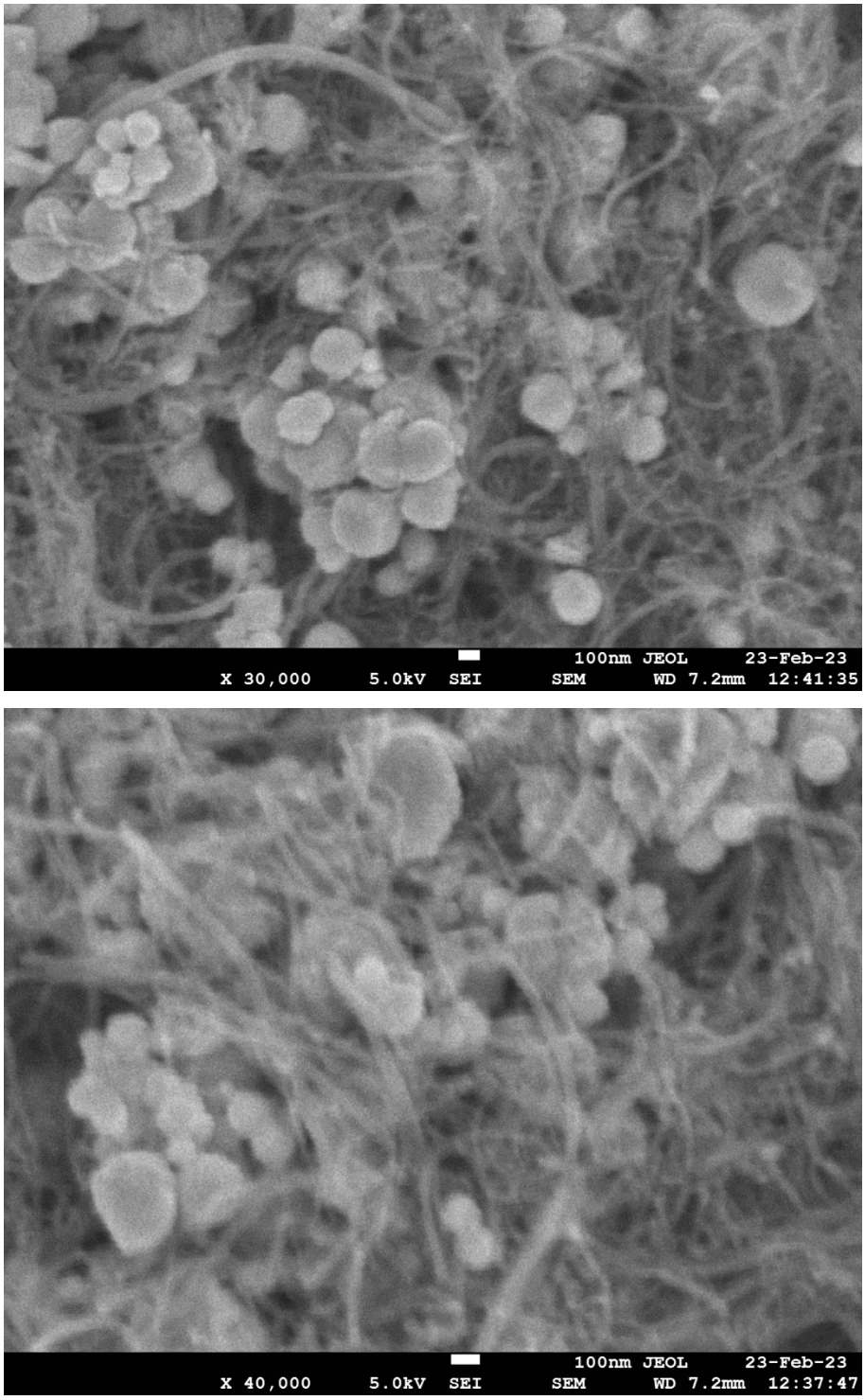

Figure S8. SEM images of f-MWCNTs/FeNPs composite.

(*a*)

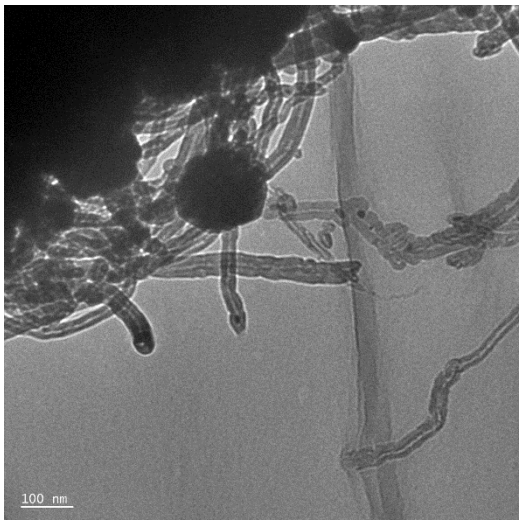

(*b*)

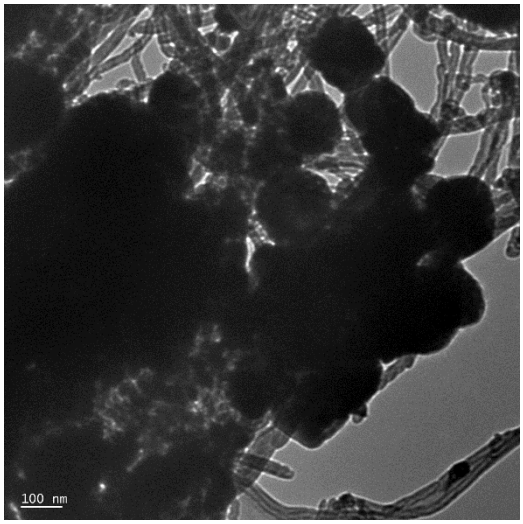

(*c*)

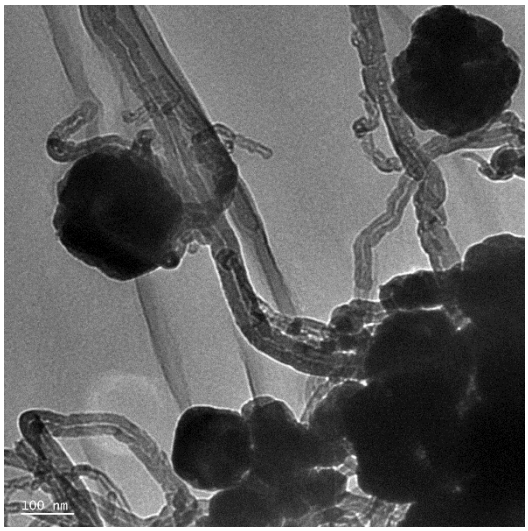

(*d*)

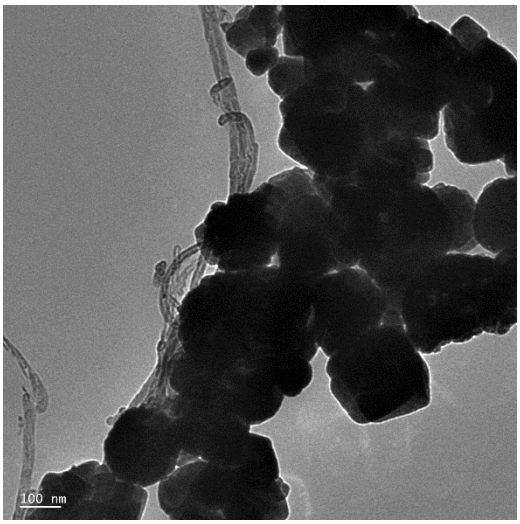

(*e*)

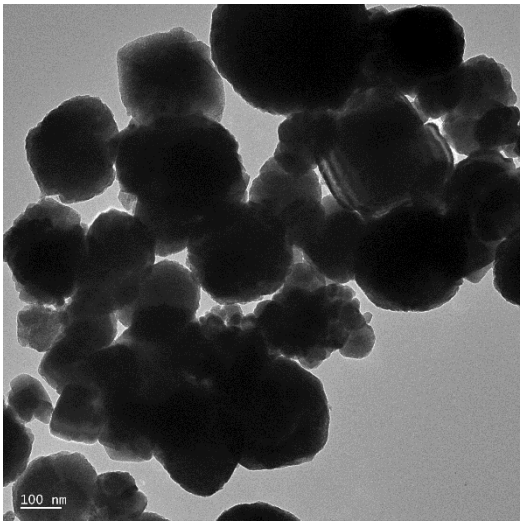

(*f*)

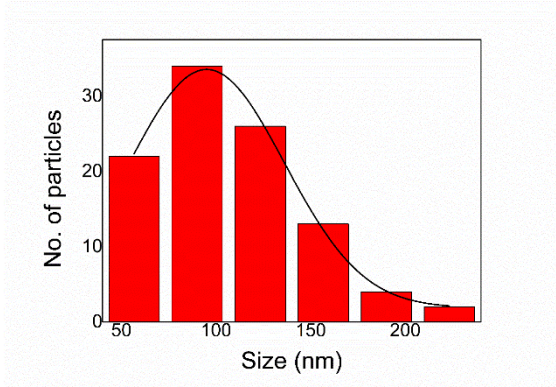

Figure S9. (*a-e*) TEM images of f-MWCNTs/FeNPs. (*f*) Size distribution histogram from TEMs. Sample size

collected: 90. Mean size: 107.2 nm. SD: 39.3 nm. Min.: 53.0 nm. Max.: 234.0 nm.

(*a*)

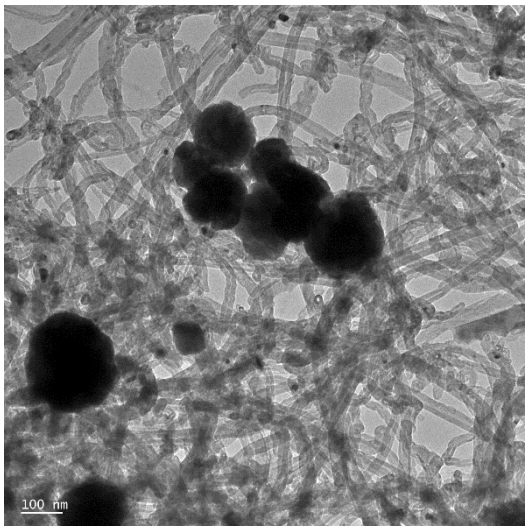

(*b*)

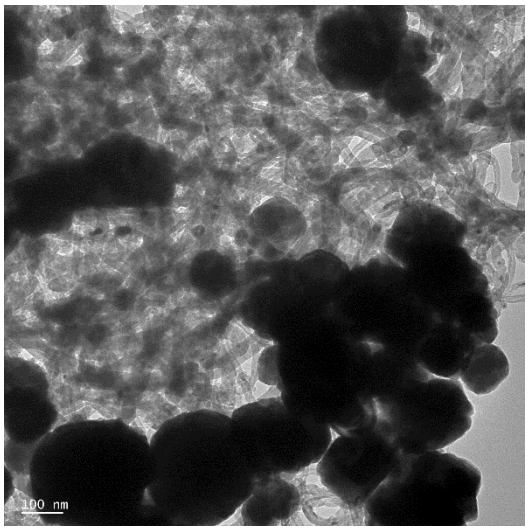

(*c*)

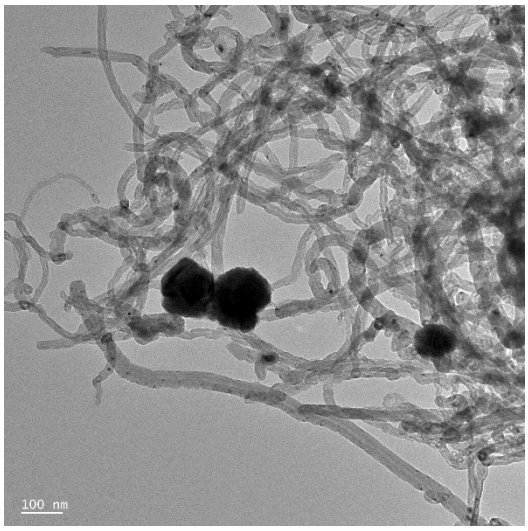

(*d*)

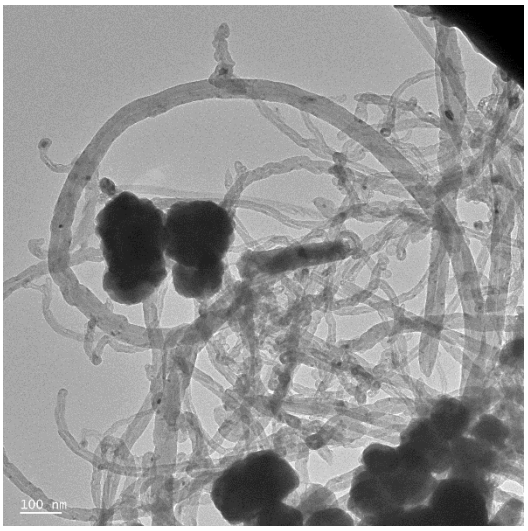

(*e*)

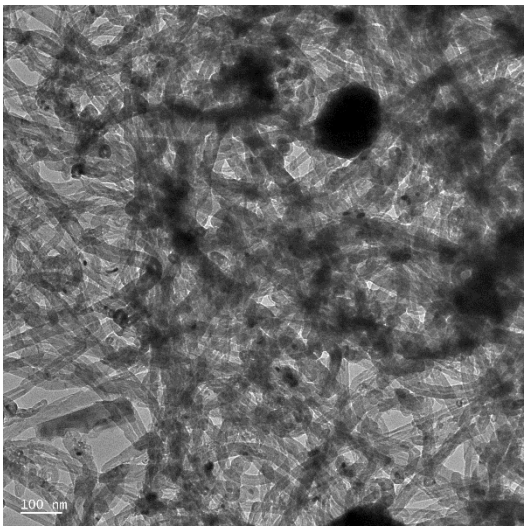

(*f*)

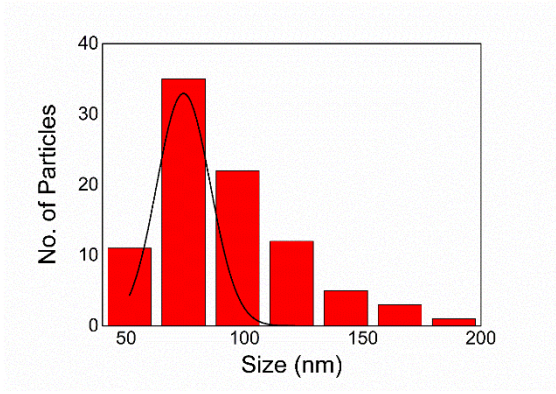

Figure S10. (*a-e*) TEM images of f-MWCNTs/FeNPs/PVP. (*f*) Size distribution histogram from TEMs. Sample size

collected: 90. Mean size: 91.1 nm. SD: 29.2
nm. Min.: 52.0 nm. Max.: 157.3 n

This is the final page of the thesis